



## Abstract

Methanol is the second-most abundant organic gas in the remote atmosphere after methane, but its sources are poorly understood. Here, we report a global budget of methanol constrained by observations from the ATom aircraft campaign as implemented in the GEOS-Chem global atmospheric chemistry model. ATom observations under background marine conditions can be fit in the model with a surface ocean methanol concentration of 61 nM and a methanol yield of 13% from the newly implemented  $\text{CH}_3\text{O}_2+\text{OH}$  reaction. While terrestrial biogenic emissions dominate the global atmospheric methanol budget, secondary production from  $\text{CH}_3\text{O}_2+\text{OH}$  and  $\text{CH}_3\text{O}_2+\text{CH}_3\text{O}_2$  accounts for 29% of the total methanol source, and contributes the majority of methanol in the background marine atmosphere sampled by ATom. Emission from the ocean is minor in comparison, particularly because of rapid deposition from the marine boundary layer. Aged anthropogenic and pyrogenic plumes sampled in ATom featured large methanol enhancements to constrain the corresponding sources. Methanol enhancements in pyrogenic plumes did not decay with age, implying in-plume secondary production. The atmospheric lifetime of methanol is only 5.3 days, reflecting losses of comparable magnitude from photooxidation and deposition. GEOS-Chem model results indicate that methanol photochemistry contributes 5%, 4%, and 1.5% of the tropospheric burdens of formaldehyde, CO, and ozone respectively, with particularly pronounced effects in the tropical upper troposphere. The  $\text{CH}_3\text{O}_2+\text{OH}$  reaction has substantial impacts on radical budgets throughout the troposphere and should be included in global atmospheric chemistry models.

## Plain Language Summary

Methanol is the most abundant non-methane organic gas in the lower atmosphere, but the magnitudes of its sources and sinks remain uncertain. Here, we evaluate a global atmospheric chemistry model against recent observations of methanol in the remote atmosphere to better constrain the methanol budget. We show that, relative to past studies, the new data suggest a smaller atmospheric methanol source from the ocean and a larger source from gas-phase chemistry. Methanol emitted from the oceans plays a particularly small role in the atmosphere because it is quickly deposited back to the ocean surface. We incorporate these updates into the global model and evaluate their importance for atmospheric chemistry more broadly, showing that methanol directly and indirectly influences the abundances of many other tropospheric trace gases.

## 1 Introduction

Methanol is the most abundant non-methane organic gas in the troposphere, where it influences the budgets of ozone and OH and is a precursor of formaldehyde and CO (Tie et al., 2003; Duncan et al., 2007; Wells et al., 2014). The dominant source of methanol to the atmosphere is its primary emission from terrestrial plants, particularly during growth and decay stages (MacDonald & Fall, 1993; Warneke et al., 1999; Galbally & Kirstine, 2002; Wohlfahrt et al., 2015; Ashworth et al., 2016). Additional sources include secondary production from the reactions of methylperoxy radicals ( $\text{CH}_3\text{O}_2$ ) with  $\text{CH}_3\text{O}_2$  and other organic peroxy radicals (Madronich & Calvert, 1990; Tyndall et al., 2001), as well as emissions from oceans (Heikes et al., 2002; Millet et al., 2008), biomass burning (e.g., Hornbrook et al., 2011; Akagi et al., 2013; Wentworth et al., 2018), and anthropogenic sources including solvent use, vehicular exhaust, and industrial processes (Olivier et al., 1994; Legreid et al., 2007; Velasco et al., 2009). Its sinks include reaction with OH (Sander et al., 2006), surface deposition (Karl et al., 2004, 2005; Talbot et al., 2005; Mao et al., 2006), and uptake by the ocean (Yang et al., 2013, 2014).

Due to its ubiquity, methanol has been the subject of many modeling studies providing estimates of its global budget in the atmosphere (Singh et al., 2000; Galbally &

78 Kirstine, 2002; Heikes et al., 2002; von Kuhlmann et al., 2003; Jacob et al., 2005; Mil-  
 79 let et al., 2008; Stavrou et al., 2011; Khan et al., 2014). While these assessments tend  
 80 to agree on the tropospheric burden of methanol (3-5 Tg), they exhibit large discrep-  
 81 ancies in total sources and sinks (90-490 Tg a<sup>-1</sup>), with even greater uncertainties for in-  
 82 dividual source terms. Comparisons with airborne observations (e.g., Singh et al., 2000;  
 83 Jacob et al., 2005; Millet et al., 2008; Müller et al., 2016), ground-based measurements  
 84 (e.g., Rinsland et al., 2009; Bader et al., 2014), and satellites (e.g., Dufour et al., 2006;  
 85 Stavrou et al., 2011; Wells et al., 2012, 2014) frequently show model biases in the sea-  
 86 sonal and spatial variations of methanol and/or model underpredictions of observed methanol  
 87 mixing ratios. Such underestimates are particularly acute in remote oceanic areas, sug-  
 88 gesting the need for additional secondary sources (Jacob et al., 2005; Stavrou et al.,  
 89 2011; Müller et al., 2016). Most recently, X. Chen et al. (2019) found that the global chem-  
 90 ical transport model GEOS-Chem underestimated methanol mixing ratios by 60% in the  
 91 boundary layer and 78% in the free troposphere over North America relative to obser-  
 92 vations from an ensemble of aircraft campaigns, accounting for nearly a quarter of the  
 93 per-carbon simulated volatile organic compound (VOC) deficit. These disparities point  
 94 to the ongoing need to better constrain the sources and sinks of tropospheric methanol.

95 An additional recently proposed source of methanol to the troposphere is the re-  
 96 action of CH<sub>3</sub>O<sub>2</sub> radicals with OH (Archibald et al., 2009; Fittschen et al., 2014), which  
 97 is hypothesized to contribute substantially to the CH<sub>3</sub>O<sub>2</sub> budget in the remote atmo-  
 98 sphere where low NO leads to long peroxy radical lifetimes:



104 The magnitude of this methanol source depends on the overall reaction rate ( $k_1 = k_{1a} +$   
 105  $k_{1b} + k_{1c} + k_{1d}$ ) and the fractional contribution of R1b to the overall reaction ( $\phi_{1b} =$   
 106  $k_{1b}/k_1$ ). Both numbers have been estimated in experimental and theoretical work but  
 107 remain poorly constrained. Measurements of  $k_1$  are in the range  $(0.8-2.8) \times 10^{-10}$  cm<sup>3</sup>  
 108 molecule<sup>-1</sup> s<sup>-1</sup> (Bossolasco et al., 2014; Assaf et al., 2016; Yan et al., 2016), while ob-  
 109 served and theoretical product yields suggest that R1a is the major pathway ( $\geq 80\%$ ),  
 110 with  $\phi_{1b}$  comprising 6-9% and R1d making up the remainder (Müller et al., 2016; As-  
 111 saf et al., 2017; Caravan et al., 2018; Yan & Krasnoperov, 2019). Modeling studies sug-  
 112 gest that values of  $k_1$  and  $\phi_{1b}$  at the upper ends of these ranges could lead to substan-  
 113 tial global methanol production (Khan et al., 2014; Ferracci et al., 2018); Müller et al.  
 114 (2016) used the upper-limit uncertainty bound of  $\phi_{1b} = 30\%$  to calculate a source strength  
 115 of 115 Tg a<sup>-1</sup>, comparable to primary terrestrial sources, which would resolve the model  
 116 underestimate in remote areas. The methanol source from the CH<sub>3</sub>O<sub>2</sub> + OH reaction  
 117 could also be modulated by the effects on reaction rates and branching ratios of com-  
 118 plexation between CH<sub>3</sub>O<sub>2</sub> and water molecules in the atmosphere, or by subsequent pro-  
 119 duction from the trioxide (CH<sub>3</sub>OOOH) in reaction channel R1d (Butkovskaya et al., 2009;  
 120 Vaida, 2011; Khan et al., 2015; Müller et al., 2016; Caravan et al., 2018). Crucially, the  
 121 CH<sub>3</sub>O<sub>2</sub> + OH reaction also competes with the methanol source from the CH<sub>3</sub>O<sub>2</sub> + CH<sub>3</sub>O<sub>2</sub>  
 122 reaction; therefore, depending on the values of  $k_1$  and  $\phi_{1b}$ , including this reaction in global  
 123 models could either decrease or increase secondary methanol production.

124 Among the other sources of methanol to the atmosphere, oceanic emissions remain  
 125 highly uncertain. Early inventories of atmospheric methanol applied a fixed saturation  
 126 ratio to the ocean surface (Singh et al., 2003; Jacob et al., 2005), effectively implying that  
 127 the supply of methanol to seawater is controlled by uptake from the atmosphere. Later  
 128 observations of sea-surface methanol indicated the presence of methanol sources and sinks  
 129 within the surface ocean (Heikes et al., 2002; Williams et al., 2004), which has since been

130 confirmed with the identification of methanol-producing phytoplankton (Mincer & Aicher,  
131 2016) and methanol-consuming microbes (e.g., Giovannoni et al., 2008). Despite the pre-  
132 sumed spatiotemporal heterogeneity of these biological controls on oceanic methanol, mea-  
133 sured sea-surface concentrations have typically been high (100-200 nM) and homogeneous,  
134 which models invoked by applying two-way methanol exchange with a single fixed sea-  
135 water concentration set to the average of past *in situ* measurements (e.g., Millet et al.,  
136 2008). However, recent studies have observed methanol concentrations an order of mag-  
137 nitude lower in the surface ocean (Yang et al., 2013, 2014) and with high interannual vari-  
138 ability (Beale et al., 2015), suggesting the need to reevaluate the oceanic contribution  
139 to atmospheric methanol.

140 In this work, we reassess the global budget of methanol by updating the GEOS-  
141 Chem model to reflect the recent advances described above and compare simulations to  
142 measurements made during the NASA Atmospheric Tomography (ATom) Mission. We  
143 correlate model-measurement disparities in the most remote regions of the troposphere  
144 with simulated tagged methanol tracers to constrain the secondary and oceanic sources,  
145 and analyze observed enhancements of methanol mixing ratios in pyrogenic and anthro-  
146 pogenic plumes to evaluate the strength of those primary emissions. With these new source  
147 estimates, we present an updated global budget of tropospheric methanol. We further  
148 describe the contribution of methanol and the newly implemented  $\text{CH}_3\text{O}_2 + \text{OH}$  reac-  
149 tion to the budgets of formaldehyde, CO, ozone, and other trace tropospheric species.

## 150 2 Methods

### 151 2.1 GEOS-Chem

152 We simulate tropospheric methanol with GEOS-Chem, a 3-D global chemical trans-  
153 port model with detailed state-of-the-science atmospheric chemistry (<http://geos-chem.org>,  
154 last access: 13 May 2020). GEOS-Chem incorporates assimilated meteorological obser-  
155 vations from the NASA Goddard Earth Observing System Fast Processing (GEOS-FP)  
156 rdata product of the NASA Global Modeling and Assimilation Office (GMAO). We use  
157 model version 11-02d including both tropospheric and stratospheric chemistry (Eastham  
158 et al., 2014) as well as updated halogen chemistry relevant to oxidant budgets in the re-  
159 mote and oceanic troposphere (Sherwen, Schmidt, et al., 2016; Sherwen, Evans, et al.,  
160 2016; Q. Chen et al., 2017). Methane mixing ratios are fixed in the model based on ob-  
161 servations. In this work, we update the chemical mechanism with improved isoprene chem-  
162 istry from Wennberg et al. (2018) using the implementation described in Bates and Ja-  
163 cob (2019). We also update the standard emissions inventories as described in the fol-  
164 lowing section, including the addition of an oceanic alkane and alkene source following  
165 Paulot et al. (2011) and Millet et al. (2015). For comparisons with flight campaigns we  
166 sample the model at the times and locations of each observation, while for annual bud-  
167 get calculations we perform simulations from 1 July 2016 to 30 June 2017. All results  
168 described herein follow a model spin-up of at least six months and are performed at  $2^\circ \times$   
169  $2.5^\circ$  horizontal resolution with 72 vertical levels.

170 We improve the diagnostic capability of GEOS-Chem by tagging methanol accord-  
171 ing to its source in order to separate the contributions from individual primary emission  
172 and secondary production sources. We add eight individual species: four representing  
173 primary biogenic, anthropogenic, pyrogenic, and oceanic methanol emissions, along with  
174 four representing secondary production of methanol from  $\text{CH}_3\text{O}_2 + \text{CH}_3\text{O}_2$ ,  $\text{CH}_3\text{O}_2 +$   
175 other organic peroxy radicals, glycolaldehyde photolysis, and the new  $\text{CH}_3\text{O}_2 + \text{OH}$  re-  
176 action. Each tagged methanol species has the same loss processes in the model as methanol  
177 itself; thus, the sum of the tagged tracers equals total methanol.

## 2.2 Model sources and sinks of methanol

For biogenic methanol emissions from living plants, we use the Model of Emissions of Gases and Aerosols from Nature (MEGAN; Guenther et al., 2012) version 2.1, described in detail by Stavrakou et al. (2011). MEGAN calculates methanol emissions ( $E$ , mol m<sup>2</sup> s<sup>-1</sup>) at each grid box and time step using the following formula:

$$E = \epsilon \times \gamma_{age} \times \gamma_{PT} \times LAI \quad (2)$$

where  $\epsilon$  represents a base emission factor dependent on plant type,  $\gamma_{age}$  is a scaling factor dependent on leaf age,  $\gamma_{PT}$  includes light- and temperature-dependent scaling, and  $LAI$  is the leaf area index. For methanol,  $\epsilon$  is set to  $6.94 \times 10^{-9}$  mol m<sup>2</sup> s<sup>-1</sup> for shrubs, crops, needle-leaf trees, and northern temperate and boreal broadleaf tree, and to  $3.47 \times 10^{-9}$  mol m<sup>2</sup> s<sup>-1</sup> for grasses and all other broadleaf trees, based on 17 observational ecosystem studies (see citations in Guenther et al., 2006; Stavrakou et al., 2011).  $\gamma_{age}$  is based on Harley et al. (2007) and Karl et al. (2003) and is highest for young leaves, which produce large amounts of methanol from pectin demethylation during their growth (MacDonald & Fall, 1993; Fall & Benson, 1996). Finally, methanol emissions are highly light- and temperature dependent (Harley et al., 2007) and drop near zero at night due to stomatal control (Nemecek-Marshall et al., 1995; Ashworth et al., 2016). In MEGAN, this is incorporated into the  $\gamma_{PT}$  factor, which parameterizes 80% of methanol emissions as light-dependent and 20% as light-independent.

Methanol is also released from dead and decaying vegetation in various biotic and abiotic demethylation processes (Galbally & Kirstine, 2002; Warneke et al., 1999). We implement this source as in Jacob et al. (2005) and Millet et al. (2008), using an emission factor of 160  $\mu$ g methanol emitted per kg dry plant mass applied to a map of heterotrophic respiration derived from the CASA 2 biosphere model (Potter et al., 1993; Randerson et al., 1997), which leads to a global methanol emission of 23 Tg a<sup>-1</sup>.

When implemented in GEOS-Chem with GEOS-FP meteorology, MEGAN tends to underestimate biogenic VOC emissions (Wells et al., 2014; Bates & Jacob, 2019), so we scale MEGAN emissions up by 10% such that the primary biogenic source (from both living and dead vegetation) is equal to 100 Tg a<sup>-1</sup>, as estimated by Stavrakou et al. (2011). While this source magnitude has also been corroborated by Millet et al. (2008) and Wells et al. (2014), multiple studies suggest that the spatiotemporal variability of methanol emissions is overly simplified by MEGAN. Rinsland et al. (2009) and Wells et al. (2014) both note a need for increased emissions from arid landscapes, and Wells et al. (2014) find that the seasonality of MEGAN emissions is biased. von Dahl et al. (2006) describe a large source from herbivory-induced plant stress that is currently absent from models. Wohlfahrt et al. (2015) review fluxes from land ecosystems and show that methanol emissions can differ substantially within plant functional types, e.g., by up to a factor of 3 for various measurements of grasslands (Fukui & Doskey, 1998; Kirstine et al., 1998; Ruuskanen et al., 2011). However, the ATom observations are not suited to discern these details in the biogenic source, so we do not address these complexities here.

Pyrogenic methanol emissions in GEOS-Chem are derived from the Global Fire Emissions Database version 4 (GFEDv4) (van der Werf et al., 2010). The calculation of gaseous emissions relies on burned area from Giglio et al. (2013) enhanced by the contribution of small fires as described in Randerson et al. (2012), with temporal scaling from Mu et al. (2011). Emission factors (g methanol emitted per kg dry material burned) for each of the six GFED4 burn types are based primarily on Akagi et al. (2011), ranging from 1.18 g kg<sup>-1</sup> for savannah fires to 8.46 g kg<sup>-1</sup> for peat fires. In GEOS-Chem, this gives an annual methanol emission of 5.9 Tg a<sup>-1</sup> in our base simulation used for initial comparisons and the regression analysis in Section 3. This is lower than previous global estimates, which range between 6 and 21 Tg a<sup>-1</sup> (Jacob et al., 2005; Millet et al., 2008; Wells et al., 2014; Andreae, 2019), but gives an average molar ratio of pyrogenic methanol emissions to those of CO of 1.85% (mol mol<sup>-1</sup>), in line with observed enhancement ra-

tios of 0.9-3.8% (Andreae & Merlet, 2001; Sinha et al., 2003, 2004; Holzinger et al., 2005; de Gouw et al., 2006; Warneke et al., 2009; Hornbrook et al., 2011; Simpson et al., 2011; Lewis et al., 2013; Li et al., 2014). As described in Section 4, we increase pyrogenic methanol emissions by a factor of 2.2 in the updated simulation for the global budgets in Section 5.

For anthropogenic methanol emissions, we use the MACCity emission dataset (Lamarque et al., 2010) which specifically includes organic alcohols as a VOC class. We implement the RCP 8.5 forward-projected anthropogenic emissions to our period of interest and assume that methanol represents 50% of alcohol emissions by carbon mass (X. Chen et al., 2019), which gives a global methanol emission of 3.15 Tg a<sup>-1</sup>, or 0.52% of CO emissions (mol mol<sup>-1</sup>) in our base simulation. This is lower than total anthropogenic methanol emissions in most previous global model budgets, which are in the range 3-8 Tg a<sup>-1</sup> (Jacob et al., 2005; Millet et al., 2008; Wells et al., 2014; Safieddine et al., 2017). As described in Section 4, we scale up anthropogenic methanol emissions by a factor of 2 in the updated simulation for the global budgets in Section 5.

The oceanic contribution to the atmospheric methanol budget is calculated locally as described by Fischer et al. (2012) for acetone in GEOS-Chem. Briefly, the parameterization is based on the two-film model of Liss and Slater (1974), by which the net flux ( $F$ , mol m<sup>-2</sup> s<sup>-1</sup>) out of the ocean can be calculated as the balance of ocean emission ( $E$ ) and uptake ( $U$ ) by the following equation:

$$F = E - U = -K_W \times (C_g \times H^{-1} - C_l) \quad (3)$$

where  $C_g$  and  $C_l$  represent the methanol concentrations in the air and water respectively,  $H$  represents the dimensionless gas-over-liquid Henry's Law equilibrium constant for methanol ( $2.02 \times 10^{-4}$ , converted from 203 M atm<sup>-1</sup> at 298 K, with a temperature dependence  $d(\ln(H))/d(1/T) = 5600$  K, from Sander et al., 2006), and  $K_W$  represents the inverse of the total transfer resistance:

$$K_W^{-1} = k_l^{-1} + (H \times k_g)^{-1} \quad (4)$$

where  $k_l$  and  $k_g$  are the wind speed-dependent liquid- and gas-phase transfer velocities, calculated using the parameterizations from Nightingale et al. (2000) and Johnson (2010) respectively. Highly soluble gases such as methanol are limited primarily by air-side transfer, with the  $k_l$  term contributing only a few percent to the overall  $K_W$  (Yang et al., 2013). The dominant  $k_g$  term is the less-studied and more uncertain element of  $K_W$ , and studies in the laboratory and field frequently disagree on its parameterization (Johnson, 2010; Yang et al., 2013). We calculate the emission and uptake terms separately such that the gross outward methanol flux can be applied to the tagged oceanic methanol tracer, while the sink to the ocean can be applied to each of the tagged methanol tracers.

Oceanic methanol is presumed to be controlled primarily by *in situ* biological activity, supported by observations of rapid production and consumption of methanol by plankton and bacteria. The *Prochlorococcus* genus of phytoplankton alone was estimated to contribute 850-1700 Tg a<sup>-1</sup> of methanol to the oceans, 10-40 times the contribution of deposition from the atmosphere (Mincer & Aicher, 2016). This source is offset by microbial uptake rates of up to 150 nM d<sup>-1</sup> (Dixon et al., 2011b), giving methanol turnover times of < 1 d. Methanol-consuming microbes have recently been observed and characterized in a wide variety of ocean environments (Dixon et al., 2011a, 2013; Dixon & Nightingale, 2012; Ramachandran & Walsh, 2015; Arrieta et al., 2016; Sargeant et al., 2016; Deng et al., 2018; Dinasquet et al., 2018), including some obligate methylophiles (Giovannoni et al., 2008), suggesting a critical role for methanol in the ocean microbiome. These various pathways of methanol production and destruction can be highly variable in both time and space. Production tends to peak only toward the end of the cell life cycle, and has been proposed to provide pulses of methanol associated with phytoplankton blooms (Mincer & Aicher, 2016). Dixon et al. (2013) and Sargeant et al. (2016) observed sharp geographic and seasonal contrasts in bacterial methanol consumption rates,

**Table 1.** Measurements of methanol in the surface ocean

Concentration <sup>a</sup> (nM)	Location	Period	Reference
118.4 ± 48.2 (60-230)	Eq. Atl.	Oct-Nov 2002	Williams et al. (2004)
158.9 ± 33.1 (78-325)	NW. Pac.	Jul-Aug 2008	Kameyama et al. (2010)
99 (<27-429)	coastal NE. Atl.	Apr-May 2009	Beale et al. (2011)
121, 137, 237, 128 <sup>b</sup>	Atlantic <sup>c</sup>	Oct-Dec 2009	Read et al. (2012)
139 ± 51 (48-361)	Atlantic <sup>c</sup>	Oct-Dec 2009	Beale et al. (2013)
49 ± 15 (16-78)	coastal NE. Atl.	Feb 2011-Mar 2012	Beale et al. (2015)
29 (15-62)	Atlantic <sup>c</sup>	Oct-Nov 2012	Yang et al. (2013)
16.3 ± 5.5 (7-28)	N. Atl.	Oct-Nov 2013	Yang et al. (2014a)
67 ± 35 (<21-226)	Southern Ocean	Feb-Apr 2020	Wohl et al. (2020)

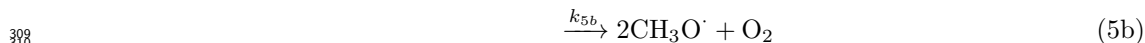
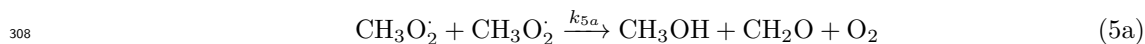
<sup>a</sup>reported values are means ± standard deviations; parentheses denote the complete range of observed values, while commas separate the means in distinct geographic regions; <sup>b</sup>values reported are means across separate latitude ranges: 30-10°S, 10°S-10°N, 10-30°N, 30-50°N; <sup>c</sup>full transect between 39°S and 49°N.

282 with different metabolic pathways (use as an energy source vs. for cell growth) domi-  
 283 nating in different regions.

284 Despite the presumed spatiotemporal heterogeneity of oceanic methanol sources  
 285 and sinks, observations of sea-surface methanol (summarized in Table 1) exhibit little  
 286 correlation with biological activity and no obvious patterns of spatial and temporal vari-  
 287 ability. Instead, there is a distinct divergence between early observations (pre-2010), which  
 288 measured concentrations of 100-240 nM, and more recent observations of < 70 nM, in-  
 289 cluding many in similar locations and seasons to the high prior observations. Past global  
 290 inventories have typically used a fixed surface seawater concentration of 118 nM, the mean  
 291 concentration observed by Williams et al. (2004), and found that the ocean provides a  
 292 gross methanol source of 43-85 Tg a<sup>-1</sup> offset by a gross sink of 48-101 Tg a<sup>-1</sup>, balanc-  
 293 ing to a net sink of 5-16 Tg a<sup>-1</sup> (Millet et al., 2008; Stavrou et al., 2011; Wells et al.,  
 294 2012, 2014). Wells et al. (2014) performed sensitivity simulations in which the seawater  
 295 concentration was varied by ±41%, which caused the net ocean sink to vary from 0  
 296 to 15 Tg a<sup>-1</sup>.

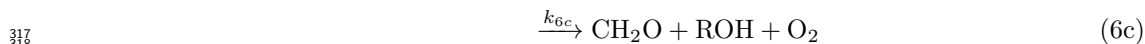
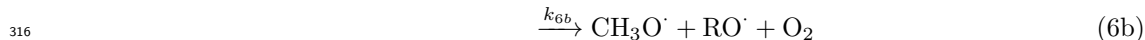
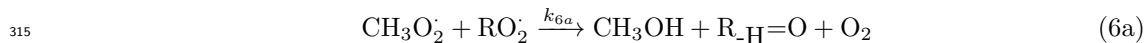
297 Here, to test the potential impact of a lower oceanic methanol concentration in line  
 298 with recent measurements, we set a fixed seawater concentration of 31.4 nM (the mean  
 299 of the three most recent Atlantic observations in Table 1) in our base simulation, which  
 300 provides a gross source term of 13 Tg a<sup>-1</sup> balanced by a computed gross sink term of  
 301 30 Tg a<sup>-1</sup>, for a net sink of 17 Tg a<sup>-1</sup>. We adjust the seawater concentration for our up-  
 302 dated simulation as described in Section 3 and find that a fixed seawater concentration  
 303 of 61 nM provides the best fit to ATom observations, which yields gross source, gross sink,  
 304 and net sink terms of 24, 38, and 14 Tg a<sup>-1</sup>.

305 Among the sources of secondary methanol in the standard GEOS-Chem mecha-  
 306 nism, the CH<sub>3</sub>O<sub>2</sub> + CH<sub>3</sub>O<sub>2</sub> reaction dominates, producing 45 Tg a<sup>-1</sup> of methanol. The  
 307 reaction proceeds by two competing pathways:



311 GEOS-Chem uses an overall rate coefficient  $k_5 = k_{5a} + k_{5b}$  of  $9.5 \times 10^{-14} \times e^{390/T}$   
 312 (Sander et al., 2006) and a temperature-dependent branching ratio of  $k_{5b}/k_{5a} = 26.2 \times$   
 313  $e^{-1130/T}$  (Tyndall et al., 2001). The methyl peroxy radical can also react with other per-

oxy radicals (represented as RO<sub>2</sub>) to produce methanol:



In GEOS-Chem, the branching ratio to methanol production ( $k_{6a}/(k_{6a}+k_{6b}+k_{6c})$ ) ranges from 20% to 50% for primary and secondary peroxy radicals, and is set to zero for tertiary and acyl peroxy radicals without available hydrogen atoms (Orlando & Tyndall, 2012). The photolysis of glycolaldehyde also produces methanol, with a yield of 10% in GEOS-Chem (Magneron et al., 2005). Together, the contributions of R6a and glycolaldehyde photolysis add only 3.2 Tg a<sup>-1</sup> of methanol to the global budget in the standard GEOS-Chem mechanism.

Here we update the GEOS-Chem chemical mechanism by adding the reaction of CH<sub>3</sub>O<sub>2</sub> with OH radicals (R1), as described in the introduction. In the base simulation, we set the reaction rate ( $k_1$ ) to the median observed value of  $1.6 \times 10^{-10}$  cm<sup>3</sup> molecule<sup>-1</sup> s<sup>-1</sup> (Assaf et al., 2016), and set the methanol yield ( $\phi_{1b}$ ) to 7%, the central estimate of both Müller et al. (2016) and Caravan et al. (2018), with the remainder forming formaldehyde + 2HO<sub>2</sub> by pathway R1a (the alkoxy intermediate shown in R1a is assumed to react promptly with O<sub>2</sub>). We then adjust the methanol yield from R1 based on ATom observations, as described in Section 3 along with additional sensitivity studies of different rates and product yields. As implemented in the base simulations, R1 provides a methanol source of 18 Tg a<sup>-1</sup>. However, because it competes as a sink for CH<sub>3</sub>O<sub>2</sub> radicals, the inclusion of R1 in GEOS-Chem decreases the methanol sources from R5 and R6 by 21 Tg a<sup>-1</sup> and 0.3 Tg a<sup>-1</sup> respectively, thus diminishing the total secondary production of methanol in the model, consistent with the results of Caravan et al. (2018). In our updated model, we find that a yield  $\phi_{1b}$  of 13% provides the optimal fit to ATom observations (see Section 3), which gives a methanol source of 33 Tg a<sup>-1</sup>.

In addition to ocean uptake described above, methanol loss processes in GEOS-Chem include reaction with OH and the chlorine radical as well as dry and wet deposition to land surfaces. The reaction of methanol with OH proceeds with a rate coefficient of  $k = 2.9 \times 10^{-12} \times e^{-345/T}$ , resulting in a globally averaged lifetime of methanol against reaction with OH of 9 d. Contradictory studies suggest that the reaction of OH with methanol may or may not be accelerated in the presence of water vapor (Jara-Toro et al., 2017; Chao et al., 2019); absent any conclusive evidence, we do not include this catalysis in our simulations. Dry deposition employs the standard GEOS-Chem resistance-in-series parameterization (Y. Wang et al., 1998), updated to account for reactive uptake by vegetation (Karl et al., 2010), resulting in a lifetime of methanol against dry deposition to land surfaces of 27 d. Wet deposition and oxidation by aqueous OH in cloud water, both unchanged from previous GEOS-Chem analyses (Jacob et al., 2005; Wells et al., 2014), and the reaction of methanol with Cl, newly implemented here with a rate constant of  $k_{Cl} = 5.5 \times 10^{-11}$  (Atkinson et al., 2006), are minor loss pathways, with associated lifetimes of 98 d, 1100 d, and 650 d respectively.

### 2.3 Observations from the NASA ATom campaign

Observations of methanol and other trace gases were conducted as part of the NASA Atmospheric Tomography (ATom) field mission. The ATom campaign included four individual deployments: July-August 2016, January-February 2017, September-October 2017, and April-May 2018. Each deployment consisted of a month-long series of flights starting and ending in Palmdale, California, during which the NASA DC-8 aircraft flew the full north-south lengths of the Pacific and Atlantic Oceans, repeatedly ascending and descending between altitudes of 200 m and 10-12 km to profile the troposphere.

364 A comprehensive suite of instruments aboard the DC-8 measured numerous trace  
 365 gases, aerosol properties, and other atmospheric quantities. Previous work comparing  
 366 these measurements to GEOS-Chem and other models have revealed the need for novel  
 367 or increased oceanic sources of many VOCs, including acetaldehyde (S. Wang et al., 2019;  
 368 Travis et al., 2020), acetone (S. Wang et al., 2020), methyl ethyl ketone (Brewer et al.,  
 369 2020), and small alkyl nitrates (Fisher et al., 2018). Even with these sources, acetalde-  
 370 hyde remains underestimated in both GEOS-Chem and CAM-Chem throughout the tropo-  
 371 sphere, suggesting the need for an unknown VOC precursor that might also contribute  
 372 to OH reactivity (S. Wang et al., 2019; Travis et al., 2020; Thames et al., 2020). Despite  
 373 this, Travis et al. (2020) found that GEOS-Chem successfully simulated tropospheric OH  
 374 to within measurement uncertainty, and that simulated  $\text{NO}_y$  was also satisfactory aside  
 375 from a high bias in wintertime  $\text{HNO}_3$  in the northern hemisphere.

376 Methanol and other organic gases discussed here, including hydrogen cyanide (HCN)  
 377 and acetonitrile ( $\text{CH}_3\text{CN}$ ), were measured with the NCAR Trace Organic Gas Analyzer  
 378 (TOGA), details of which can be found in previous publications (Apel et al., 2003, 2010;  
 379 Hornbrook et al., 2011; Apel et al., 2015). TOGA combines a cryogenic preconcentra-  
 380 tor, a gas chromatograph (Restek MXT 624 8-m column, 0.18 mm inner diameter), and  
 381 an Agilent 5973N mass spectrometer to measure mixing ratios of numerous VOCs. TOGA  
 382 has a total sample throughput time of two minutes, which enabled 11,517 individual ob-  
 383 servations of methanol (and other VOCs) over the course of the four ATom deployments.  
 384 The precise inlet configuration and other details of the TOGA setup in ATom can be found  
 385 in S. Wang et al. (2019). Precision and accuracy for the detection of methanol by TOGA  
 386 were estimated at 10 pptv and 30% respectively. Inorganic gases used in the present anal-  
 387 ysis include CO measured by Quantum Cascade Laser Spectrometer (QCLS) and wa-  
 388 ter vapor measured with a Diode Laser Hygrometer (DLH) (Diskin et al., 2002; McManus  
 389 et al., 2005), both averaged to the same observation frequency as the TOGA measure-  
 390 ments. For periods when the QCLS was calibrating, CO measurements with a Picarro  
 391 Analyzer were used instead, corrected for difference from the QCLS with a low-pass fil-  
 392 ter.

### 393 3 Constraints on secondary and oceanic methanol sources

394 Figures 1 and S1 show measured methanol mixing ratios along the ATom flight tracks.  
 395 ATom observations, as with previous campaigns, exhibit a persistent high methanol back-  
 396 ground of several hundred pptv throughout the troposphere. The highest mixing ratios  
 397 (several ppbv) are encountered over North America in summer, when biogenic emissions  
 398 peak (Wells et al., 2012), and in biomass burning plumes frequently observed during At-  
 399 lantic transects. The lowest levels (tens of pptv) are found in the stratosphere and in the  
 400 high latitudes during winter months. There is pronounced seasonal variability at high  
 401 northern latitudes and southern mid-latitudes (high in spring-summer, low in winter),  
 402 but variability elsewhere is driven primarily by the interception of continental plumes.

403 Figures 1-3 show comparisons between GEOS-Chem simulations and ATom obser-  
 404 vations as functions of latitude, altitude, and region. While the model generally captures  
 405 the features of the methanol altitude profiles and seasonal cycles (see Figures S2-S3) both  
 406 globally and regionally, the base model (in gray) exhibits a substantial negative bias, un-  
 407 derestimating methanol globally by over 50% (normalized mean bias, NMB). The model  
 408 bias is largest in the Arctic, where it exceeds 70%, and in the northern mid-latitudes,  
 409 except during winter; it is smallest in equatorial regions and over the Southern Ocean.  
 410 Only over the Southern Ocean in austral winter does the base model overestimate the  
 411 tropospheric methanol column. Averaged across seasons, however, the negative model  
 412 bias exceeds 30% everywhere, suggesting a ubiquitously underestimated methanol source  
 413 throughout the troposphere.

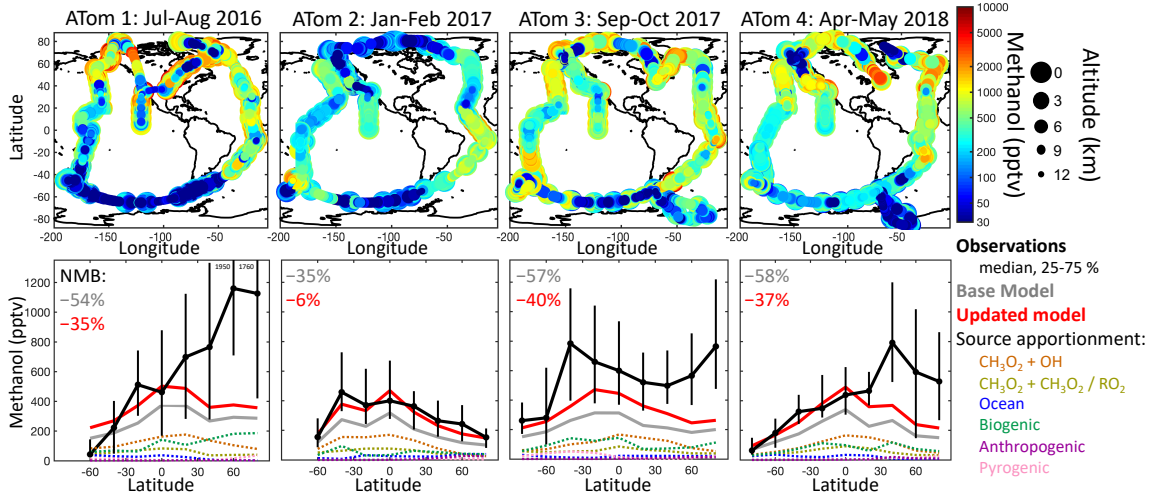


**Figure 1.** Methanol concentration during ATom. Top panels show measured methanol along the ATom flight tracks; point colors correspond to the methanol mixing ratio, while point size corresponds to altitude. Bottom panels show simulated and measured methanol as a function of latitude for each ATom mission. Measurement medians along with 25-75 percentile ranges are shown in black, while medians from the base and updated models are shown in gray and red respectively, and source contributions from the updated model are shown in colored dashed lines, all binned by 20° latitude intervals.

On a global scale, the negative model bias is strongly correlated with HCN, benzene, and CO (see Figure S4), suggesting that pyrogenic, anthropogenic, and potentially biogenic sources are underestimated. However, these biases from terrestrial sources might be caused by a number of factors that are difficult to disentangle because ATom provided only limited and indirect information on source regions. Here, we seek to isolate the observations remote from continental influence in order to focus on the highly uncertain  $\text{CH}_3\text{O}_2 + \text{OH}$  and oceanic contributions to the budget, which will enable us to fit the measurement-model difference with the following equation:

$$\text{CH}_3\text{OH}_{\text{TOGA},i} - \text{CH}_3\text{OH}_{\text{base},i} = \alpha \times \text{CH}_3\text{OH}_{\text{OH},i} + \beta \times \text{CH}_3\text{OH}_{\text{ocean},i} + \epsilon_i \quad (7)$$

where  $\text{CH}_3\text{OH}_{\text{TOGA},i}$  represents the methanol mixing ratio measured by TOGA at point  $i$ ,  $\text{CH}_3\text{OH}_{\text{base},i}$  represents the base simulated methanol at that point, and  $\text{CH}_3\text{OH}_{\text{OH},i}$  and  $\text{CH}_3\text{OH}_{\text{ocean},i}$  represent the tagged methanol from the  $\text{CH}_3\text{O}_2 + \text{OH}$  and oceanic sources respectively. We then find the values of the coefficients  $\alpha$  and  $\beta$ , constrained to stay above -1 to avoid negative source terms, that minimize the sum of the squared errors  $\epsilon_i$ ; the resulting coefficients represent the scaling factors that need to be applied to the  $\text{CH}_3\text{O}_2 + \text{OH}$  and oceanic sources in order to minimize the model underestimate. The  $\text{CH}_3\text{O}_2 + \text{OH}$  and oceanic methanol sources exhibit little collinearity (variance inflation factor = 1.08). Key assumptions and uncertainties inherent to this approach are discussed at the end of the section.

To isolate remote tropospheric points, we exclude from the present analysis any TOGA observations over land, stratospheric points (those with measured water vapor below 15 ppmv), as well as points for which benzene, CO, and HCN exceed certain background thresholds. We vary these thresholds to find a combination that includes the maximum number of observations while minimizing the correlations with CO, HCN, and benzene (determined by separately adding terms for each species to the fit in Equation 7, e.g.,  $\delta \times \text{CO}_{\text{obs},i}$ , and finding the corresponding coefficient  $\delta$  indistinguishable from or less

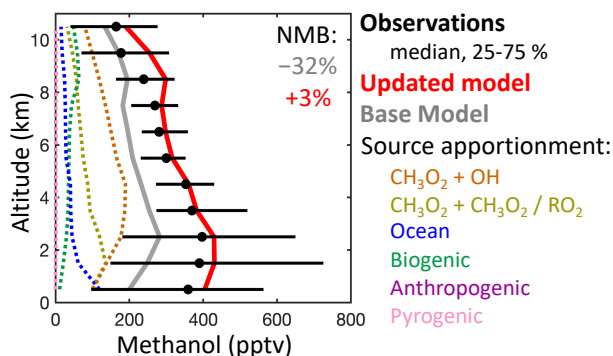


**Figure 2.** Altitude profiles of measured and simulated remote methanol mixing ratios during ATom. Measurement medians along with 25-75 percentile ranges are shown in black, while medians from the base and updated models are shown in gray and red respectively, and source contributions from the updated model are shown in colored dashed lines, all binned by 1 km altitude intervals.

440 than zero at the 95% confidence level). The resulting threshold values are 3 ppbv for ben-  
 441 zene, 200 pptv for HCN, and a latitude-dependent CO background rising linearly from  
 442 60 ppbv at and below 45°S to 120 ppbv at and above 45°N. This results in 1,861 remote  
 443 TOGA samples to use in the fit in Equation 7. The coefficient estimates described be-  
 444 low are insensitive to moderate changes in the precise choice of background threshold;  
 445 for example, increasing any of the threshold mixing ratio values by 20%, replacing the  
 446 HCN threshold with CH<sub>3</sub>CN, or replacing the latitude-dependent CO threshold with a  
 447 fixed threshold of 100 ppbv all result in coefficient estimates that are not statistically dif-  
 448 ferent from those we report here.

449 After isolating the remote points, we find that the best fit in Equation 7 gives co-  
 450 efficients of  $\alpha = 0.88 \pm 0.06$  and  $\beta = 0.94 \pm 0.09$  (reported error bounds are standard  
 451 deviation estimates using the bootstrapping method). Applying these coefficients to the  
 452 CH<sub>3</sub>O<sub>2</sub> + OH and oceanic methanol sources respectively removes the negative model bias  
 453 for remote points, as shown in Figure 2, and reduces the absolute mean error (AME) and  
 454 root mean squared error (RMSE) by 25% (see Figure S5). Applying these coefficients  
 455 to the full ATom dataset reduces the model bias from -56% to -31% and brings the sim-  
 456 ulated methanol mixing ratios in the equatorial regions and over the Southern Ocean to  
 457 within 15% of the measured values, when averaged across seasons (Figure 3d, f, h). How-  
 458 ever, methanol remains underestimated by the model in parts of the troposphere influ-  
 459 enced by continental sources. This underestimate is most pronounced in the northern  
 460 mid- and high latitudes (Figure 3a-c), except during winter, suggesting that Northern  
 461 Hemispheric terrestrial methanol sources remain underestimated in the updated model.  
 462 This will be addressed in Section 4.

463 The values of the coefficients  $\alpha$  and  $\beta$  imply a branching ratio of methanol forma-  
 464 tion from the CH<sub>3</sub>O<sub>2</sub> + OH reaction of  $\phi_{1b} = 13.2 \pm 0.4\%$  and a uniform oceanic sur-  
 465 face methanol concentration of  $61 \pm 3$  nM. While a 13% methanol yield through Reac-  
 466 tion R1b is larger than the most recent experimental estimates (Caravan et al., 2018),  
 467 it remains within the uncertainty bounds of measured total methanol formation from Re-  
 468 action R1, including possible contributions from an increased rate or from secondary forma-  
 469 tion via the trioxide (R1d). Indeed, the overall methanol yield from Reaction R1 es-  
 470 timated by Müller et al. (2016), including via R1d, totals 11.5%. We test these possi-  
 471 bilities with two sensitivity simulations, identical to the base simulation but with (a) a

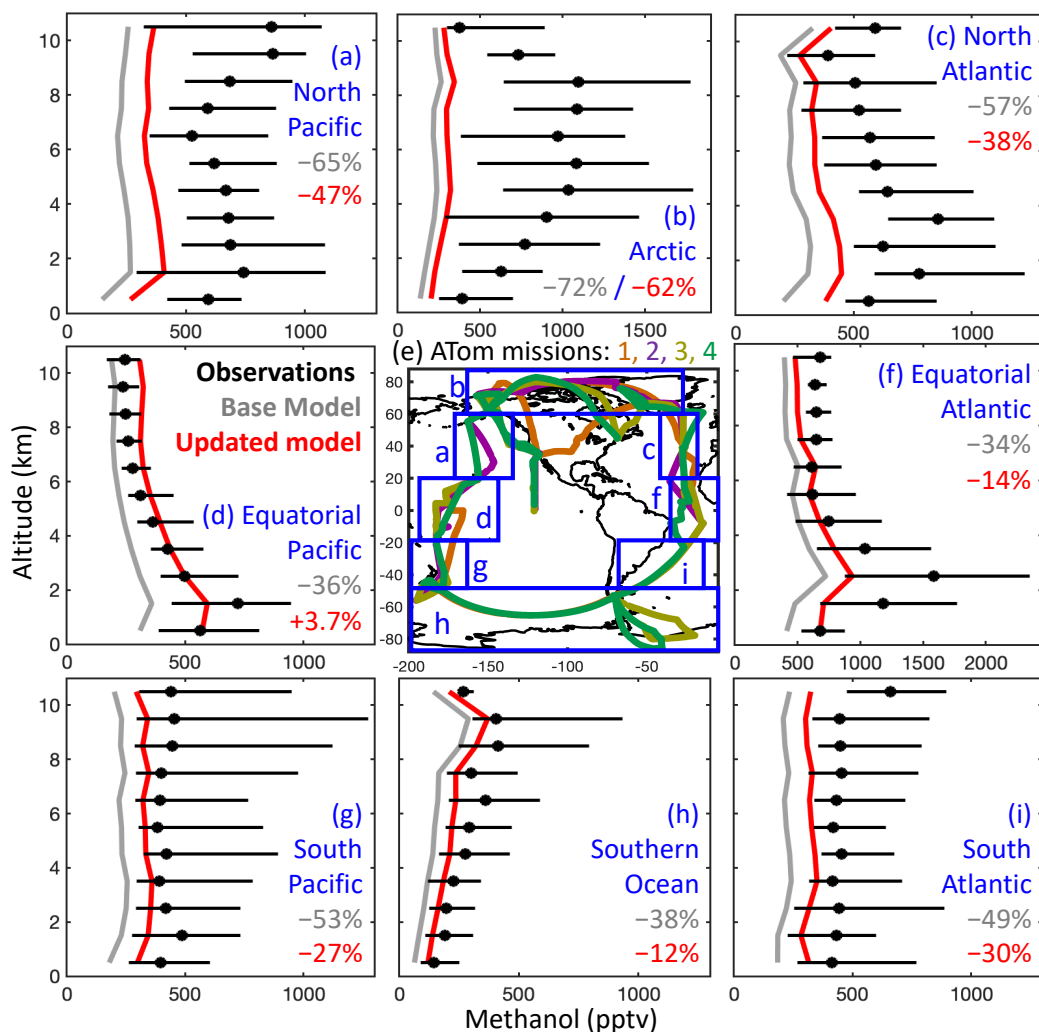


**Figure 3.** Regional altitude profiles of measured and simulated methanol mixing ratios during ATom. Measurement medians along with 25-75 percentile ranges are shown in black, while medians from the base and updated models are shown in gray and red respectively. Regional boundaries and ATom flight tracks are shown on the map at center (e). Altitude scales are identical between panels, but methanol scales differ.

472 faster  $k_1$  rate ( $2.8 \times 10^{-10} \text{ cm}^3 \text{ molecule}^{-1} \text{ s}^{-1}$ ), causing decreased methanol produc-  
 473 tion from  $\text{CH}_3\text{O}_2 + \text{CH}_3\text{O}_2$  but increased production from  $\text{CH}_3\text{O}_2 + \text{OH}$ , and (b) the  
 474 addition of channel d to Reaction R1, forming the trioxide  $\text{CH}_3\text{OOOH}$ , which reacts as  
 475 in Müller et al. (2016) to form additional methanol, such that the total methanol yield  
 476 is 13%. Refitting Equation 7 with the output of these simulations results in a worse fit  
 477 for case (a) (lower  $R^2$ , higher AME and RMSE) and an indistinguishable fit for case (b).  
 478 Thus, we cannot determine from our simulations whether methanol production from  $\text{CH}_3\text{O}_2$   
 479 + OH is prompt or proceeds through a trioxide intermediate, but we achieve the best  
 480 fit to methanol observations with an overall yield of 13%.

481 Our inferred ocean concentration of 61 nM is within the bounds of previous mea-  
 482 surements, and closer to the recent low values observed by Yang et al. (2013), Yang et  
 483 al. (2014b), and Beale et al. (2015). While it is nearly 50% lower than the value of 118

484 nM used in previous global models, which was prescribed on the basis of early measure-  
 485 ments by Williams et al. (2004), the resulting net global flux of methanol ( $14 \text{ Tg a}^{-1}$  from  
 486 the atmosphere to the ocean), shown in Figure 4, is comparable in magnitude and spa-  
 487 tial variability to previous budgets (e.g., Figure 3 in Millet et al., 2008). Indeed, our con-  
 488 straint on the oceanic contribution to atmospheric methanol is predominantly on the net  
 489 flux, while the seawater methanol concentration we derive from our fitting is highly sen-  
 490 sitive to the air-sea exchange parameterization scheme. We test this by performing a sen-  
 491 sitivity simulation in which we replace the methanol uptake term in Equation 3 with the  
 492 generic dry deposition scheme from GEOS-Chem and refit Equation 7 with the result-  
 493 ing output. While deposition to the ocean decreases by a factor of two, we find that the  
 494 coefficient  $\beta$  drops in tandem to give a comparable net oceanic flux and quality of fit,  
 495 providing confidence that our inferred flux values are well-constrained. Furthermore, our  
 496 inferred ocean fluxes across the low-to-mid-latitude Atlantic of  $3\text{-}10 \mu\text{mol m}^{-2} \text{ d}^{-1}$  (Fig-  
 497 ure 4b) are comparable to the only *in situ* flux observations available, which measured  
 498 mean values of  $8.0$  and  $12.5 \mu\text{mol m}^{-2} \text{ d}^{-1}$  in the Southern and Northern Hemispheric  
 499 Atlantic respectively (Yang et al., 2014) and  $15 \mu\text{mol m}^{-2} \text{ d}^{-1}$  in the Northwest Atlantic  
 500 (Yang et al., 2014b).

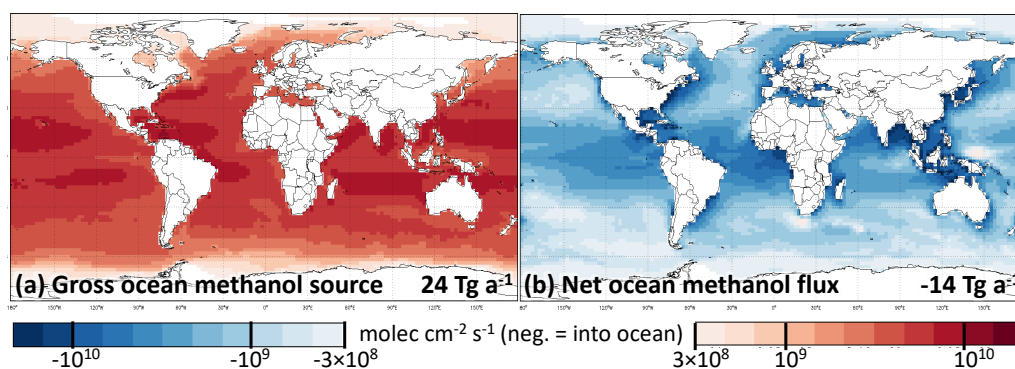


**Figure 4.** Simulated ocean-atmosphere methanol exchange. The left panel shows annual average gross methanol emissions from the ocean, while the right panel shows the annual average net flux of methanol from the ocean to the atmosphere, both in the updated simulation. Negative fluxes in the right panel indicate net uptake.

501 The formulation of Equation 7 prescribes a uniform correction factor for the con-  
 502 centration of methanol in the surface ocean, but can be reformatted to estimate correc-  
 503 tion factors that vary in space and time. Instead of fitting a single  $\beta$  coefficient, we can  
 504 fit a vector  $\vec{\beta}$  which applies a different coefficient to oceanic methanol in each ocean basin  
 505 and season. We test this by splitting the ocean source term by ATom mission and by the  
 506 regions shown in Figure 3 (excluding the Arctic, which lacks sufficient remote points)  
 507 and refitting Equation 7, constraining all coefficients to be greater than -1. This gives  
 508  $\alpha = 0.85 \pm 0.04$  (not significantly different from the fixed-ocean fit), while giving surface  
 509 seawater methanol concentrations between 0 and 300 nM. While these values fall within  
 510 measured ranges, the overall fit between the model and observations is not substantially  
 511 improved, and few of the individual oceanic coefficients are sufficiently constrained to  
 512 be significantly different from the fixed value. For completeness, we show the variable-  
 513 ocean profiles as dashed lines in Figures S2-S3 and provide the inferred concentrations  
 514 in Table S1, but we continue to use the fixed-ocean simulations for the rest of the present  
 515 analysis.

516 Even allowing for a variable ocean concentration, the linear fitting method used  
 517 here includes a number of inherent assumptions: first, that the total simulated methanol

will respond linearly to perturbations in the sources; second, that the  $\text{CH}_3\text{O}_2+\text{OH}$  and oceanic terms are parameterized correctly, requiring only linear modifications; and third, that the  $\text{CH}_3\text{O}_2+\text{OH}$  and oceanic terms are the only sources responsible for the model bias. We see little reason to assume the first assumption does not hold, as minor modifications to the methanol budget should not cause non-linear behavior such as a strong reduction in OH (see Section 5.1). We have already described sensitivity studies designed to test the second assumption (e.g., varying the  $k_1$  rate, implementing a trioxide intermediate in the  $\text{CH}_3\text{O}_2+\text{OH}$  reaction, and testing ocean deposition schemes), from which we conclude that, while plausible, these changes to the source parameterizations would not substantially change our inferences about the contributions of these sources to the methanol budget.

We test the third assumption – that the  $\text{CH}_3\text{O}_2+\text{OH}$  and oceanic terms are the only sources that contribute to the model bias in the remote troposphere – in two ways. First, we add terms to Equation 7 for each of the six other tagged tracers from the simulation and refit the model-measurement difference for remote points. Each of the terms result in coefficients indistinguishable from or equal to zero. Second, we perform a sensitivity simulation in which we increase the rate of the reaction between OH and methanol by 5%, to test whether perturbations to the methanol sink might influence the results. Refitting Equation 7 using the results of this simulation, with or without the additional tagged tracers, results in an indistinguishable fit with a slightly smaller coefficient  $\alpha$  (within uncertainty). Between these tests and eliminating the correlations of the model bias with CO, HCN, and benzene, we believe we have isolated the parts of the atmosphere where only the  $\text{CH}_3\text{O}_2+\text{OH}$  and oceanic sources contribute to the bias; however, we cannot rule out the possibility that additional sources not considered here, such as secondary production from another methyl peroxy reaction pathway or from additional ocean-derived VOCs, may play a role. This would cause our coefficients  $\alpha$  and  $\beta$  to be overestimated. However, our updated simulation would still have the correct approximate total source strength in the remote troposphere for the purposes of global budget estimates (Section 5); the source would just be erroneously attributed to the  $\text{CH}_3\text{O}_2+\text{OH}$  and oceanic terms instead of any unidentified source we exclude.

#### 4 Plume-based constraints on terrestrial sources

Despite its focus on the remote atmosphere, the ATom mission sampled a number of strong terrestrial plumes. Our ability to diagnose the model-measurement disparity in these plumes from the regression analysis used in Section 3 is limited for at least two reasons. First, global-scale plume transport in Eulerian models is hampered by fast numerical diffusion in sheared or divergent flows (Eastham & Jacob, 2017; Zhuang et al., 2018). Second, the model bias in terrestrial source strength is likely highly heterogeneous; using a fitting procedure as in Equation 7 to constrain terrestrial sources would fail to account for this heterogeneity, as it assumes the spatiotemporal pattern of methanol emissions is correct and only requires linear scaling.

Instead, we examine the potential for the ATom dataset to provide constraints on pyrogenic and anthropogenic methanol emissions by isolating individual plumes and comparing their elevated levels of methanol to previous measurements and to the emission ratios used in GEOS-Chem. Our metric for comparison is the normalized excess mixing ratio (NEMR), calculated as:

$$NEMR = 1000 \times \frac{\Delta[\text{CH}_3\text{OH}]}{\Delta[\text{CO}]} = \frac{[\text{CH}_3\text{OH}]_{\text{plume}} - [\text{CH}_3\text{OH}]_{\text{background}}}{[\text{CO}]_{\text{plume}} - [\text{CO}]_{\text{background}}} \quad (8)$$

We identify plumes as in Hornbrook et al. (2011), isolating periods of sharply delineated increases in CO and methanol, and selecting the closest available unelevated samples at a similar altitude as a background. Details for individual plumes are reported in Tables S2-S3. We categorize plumes as pyrogenic if they are accompanied by elevated HCN and

568  $\text{CH}_3\text{CN}$  ( $\text{NEMR}_{\text{CH}_3\text{CN}:\text{CO}} > 1.5$ ), and anthropogenic if not. Unfortunately, a lack of ex-  
 569 clusively biogenic tracers in continental plumes observed during ATom precludes quan-  
 570 tification of biogenic methanol emissions. The selected backgrounds may differ from the  
 571 continental boundary layer backgrounds of methanol and CO, adding large uncertainty  
 572 to the calculated NEMR (Mauzerall et al., 1998). In addition, pyrogenic and anthropogenic  
 573 sources of methanol and CO are likely to coincide with biogenic emissions, which may  
 574 then be misattributed. To minimize this interference, we isolate only the wintertime an-  
 575 thropogenic plumes for further analysis; we do not find a significant seasonal difference  
 576 in NEMR for pyrogenic plumes, which are generally more distinct (higher mixing ratio  
 577 enhancements above background) than anthropogenic plumes. We calculate the methanol  
 578 NEMR individually for each of the 20 identified pyrogenic and 6 wintertime anthropogenic  
 579 plumes, then use as our central estimate the mean NEMR across plumes, weighted both  
 580 by the error-propagated standard deviation in the plume NEMR and the number of points  
 581 per plume.

582 Figure 5a shows the CO and methanol enhancements of individual plumes along  
 583 with the weighted mean NEMRs for pyrogenic and wintertime anthropogenic plumes,  
 584 for which we find values of  $39.8 \pm 13$  ppt  $\text{ppb}^{-1}$  and  $10.4 \pm 2.1$  ppt  $\text{ppb}^{-1}$  respectively.  
 585 Our observed pyrogenic NEMR is higher than most previous measurements (10-31; Lewis  
 586 et al., 2013; Li et al., 2014; Hornbrook et al., 2011, and references therein), but not im-  
 587 plausible; Holzinger et al. (2005) measured a methanol:CO NEMR of 38 ppt  $\text{ppb}^{-1}$  in  
 588 aged biomass burning plumes over the Eastern Mediterranean. It suggests that the GFED-  
 589 derived methanol:CO emission ratio of 1.85% in GEOS-Chem should be increased by a  
 590 factor of 2.2, which brings the total pyrogenic methanol emissions into the range of pre-  
 591 vious model estimates (Section 5); other recent assessments of both GEOS-Chem and  
 592 GFED have similarly suggested that the currently implemented emission ratios fall short  
 593 of observations (Wells et al., 2014; Andreae, 2019). Our observed wintertime anthropogenic  
 594 NEMR falls well within the range of observations (8.4-22; Goldan et al., 1995; Holzinger  
 595 et al., 2001; de Gouw et al., 2005; Warneke et al., 2007; Borbon et al., 2013; Karl et al.,  
 596 2018), and suggests that the the current methanol:CO emission ratio of 0.52% in GEOS-  
 597 Chem should be increased by a factor of 2, as similarly found by a recent study of field  
 598 campaigns above North America (X. Chen et al., 2019). As with the pyrogenic source,  
 599 this increase brings the total anthropogenic methanol emissions in GEOS-Chem into the  
 600 range of previous model estimates.

601 The NEMR may differ from the methanol:CO emission ratio due to chemical pro-  
 602 duction and loss of methanol and CO in the plume during the interval between emission  
 603 and sampling. Past studies have noted that the methanol NEMR may increase with time,  
 604 likely due to secondary production in pyrogenic plumes (Holzinger et al., 2005; Akagi  
 605 et al., 2013), although contradictory evidence exists for this source (Bruns et al., 2017).  
 606 We do not observe a statistically significant dependence of methanol NEMR on plume  
 607 age (Figure 5b), suggesting that secondary methanol production must occur in plumes  
 608 to balance its faster oxidative loss than CO (by a factor of 4 at 298 K). Using only fresh  
 609 ( $< 10$  d) plumes for our analysis gives weighted mean pyrogenic and anthropogenic NEMRs  
 610 indistinguishable within uncertainty from the weighted means unfiltered by plume age,  
 611 which supports our use of the NEMR to adjust the GEOS-Chem emission ratios.

## 612 5 The global methanol budget

613 Table 2 shows the global annual budget of tropospheric methanol from our updated  
 614 simulation, after implementing the changes to methanol source terms described in Sec-  
 615 tions 3-4, along with comparisons to global budgets from previous studies. Figure 6 shows  
 616 the contributions of methanol from individual sources to the total tropospheric burden;  
 617 corresponding zonal profiles, maps of emissions, and maps of the percent contribution  
 618 from each source can be found in Figures S6-S9. We find that biogenic terrestrial emis-  
 619 sions constitute nearly half of the tropospheric source and burden of methanol, while sec-

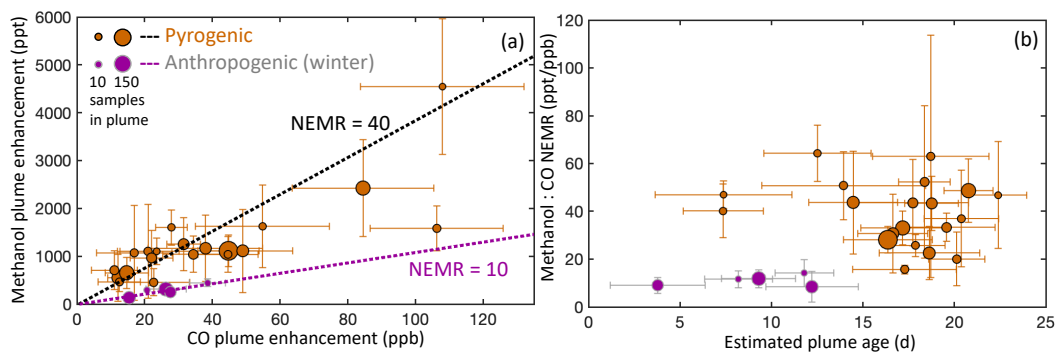


**Figure 5.** Pyrogenic and anthropogenic plumes in ATom. (a) Methanol and CO enhancements above background in each sampled plume; points are sized by the number of observations, and lines represent weighted mean methanol:CO NEMRs for all pyrogenic plumes and for wintertime anthropogenic plumes. (b) Methanol:CO NEMRs and estimated ages (from back-trajectories; see Supporting Information) of each sampled plume. Error bars represent the propagated error from the standard deviations of methanol and CO observations and estimated plume age in each plume and background sample, and do not include the instrumental uncertainty or uncertainty in individual plume age estimates.

620 onduary production contributes another  $\sim 30\%$ . We calculate the total sources and sinks  
 621 of methanol to be  $205 \text{ Tg a}^{-1}$ , within 5% of the median of previous estimates despite  
 622 our changes to individual source terms. Our atmospheric methanol lifetime of 5.3 d and  
 623 burden of  $3.0 \text{ Tg}$  are on the lower ends of the ranges of previous estimates. A more de-  
 624 tailed listing of methanol budgets from previous studies is provided in Table S4.

625 The most prominent change to our methanol budget relative to previous work is  
 626 the increased importance of secondary methanol production, predominantly from the in-  
 627 clusion of the  $\text{CH}_3\text{O}_2 + \text{OH}$  reaction, which we find provides the second largest contri-  
 628 bution to tropospheric methanol behind biogenic emissions. Despite the corresponding  
 629 decreased methanol production from the  $\text{CH}_3\text{O}_2 + \text{CH}_3\text{O}_2$  reaction, we find a total sec-  
 630 ondary methanol source of  $60 \text{ Tg a}^{-1}$ , 60% larger than the median from previous bud-  
 631 gets. Müller et al. (2016), the only other study to incorporate an appreciable methanol  
 632 source from the  $\text{CH}_3\text{O}_2 + \text{OH}$  reaction, found a similar total secondary methanol pro-  
 633 duction of  $59 \text{ Tg a}^{-1}$ . Jacob et al. (2005) proposed that a secondary methanol source  
 634 of  $50\text{-}100 \text{ Tg a}^{-1}$ , higher than mechanisms known at the time could provide, would al-  
 635 leviate negative model biases over the tropical Western Pacific. Thus, our increased sec-  
 636 ondary contribution to the methanol budget remains consistent with previous work.

637 The other notable change to the methanol budget introduced here is the reduced  
 638 gross oceanic source due to our lower seawater methanol concentration and updated pa-  
 639 rameterization of transfer velocities. While we simulate a similar small net flux of methanol  
 640 to the ocean ( $14 \text{ Tg a}^{-1}$ ) to previous studies (median  $10 \text{ Tg a}^{-1}$ ), our gross oceanic emis-  
 641 sion of  $24 \text{ Tg a}^{-1}$  is only 60% as large as the median of previous estimates and 30% as  
 642 large as in Millet et al. (2008). This also causes a strong reduction in the gross uptake  
 643 of methanol by the ocean, because most ocean-derived methanol is rapidly lost again to  
 644 the sea surface. Because of this rapid oceanic uptake, equivalent to a mean deposition  
 645 velocity of  $0.67 \text{ cm s}^{-1}$  across the ocean surface, the ocean-derived methanol has a short  
 646 lifetime and is a minor contributor to the methanol budget even in the marine bound-  
 647 ary layer, where the secondary source (including subsiding from above) dominates (see  
 648 Figure 2). Indeed, we find that the atmospheric lifetime of ocean-derived methanol (3.2

**Table 2.** Global budget of atmospheric methanol

	Previous estimates <sup>a</sup>	This work <sup>b</sup>
All sources (Tg a <sup>-1</sup> )	214 (105-287)	205
Terrestrial biogenic <sup>c</sup>	110 (95-230)	101
Biogenic growth	100 (75-280)	78
Biogenic decay	20 (13-23)	23
Anthropogenic	4.5 (1-9.3)	6.3
Pyrogenic	11 (4.3-13)	13
Oceanic <sup>d</sup>	43 (30-85)	24
Secondary production <sup>c</sup>	37 (18-48)	60
CH <sub>3</sub> O <sub>2</sub> + CH <sub>3</sub> O <sub>2</sub>	31 (15-48)	24
CH <sub>3</sub> O <sub>2</sub> + OH <sup>e</sup>	18 (8-44)	33
Other reactions <sup>e</sup>	3.0	3.0
All sinks (Tg a <sup>-1</sup> )	214 (105-299)	205
Reaction with OH	104 (66-218)	114
Reaction with Cl <sup>f</sup>	1.4	1.7
Ocean uptake <sup>d</sup>	61 (10-101)	38
Wet deposition	11 (2.7-13)	11
Dry deposition to land	34 (24-70)	41
In-cloud oxidation	<1 (0-10)	<1
Lifetime (d)	6.6 (4.7-12)	5.3
Burden (Tg)	3.4 (2.9-5)	3.0

<sup>a</sup>Median and range of central estimates from the following previous global budget analyses: Singh et al. (2000), Galbally and Kirstine (2002), Heikes et al. (2002), von Kuhlmann et al. (2003), Tie et al. (2003), Jacob et al. (2005), Millet et al. (2008), Stavrou et al. (2011), Wells et al. (2014), Khan et al. (2014), and Müller et al. (2016); <sup>b</sup>global GEOS-Chem budget from our updated simulation; <sup>c</sup>subcategories do not sum to category totals because they only include those studies that specify the biogenic and secondary pathways; <sup>d</sup>including only those studies that report gross oceanic emissions and uptake, rather than net values; <sup>e</sup>only Müller et al. (2016) and Khan et al. (2014) included the CH<sub>3</sub>O<sub>2</sub>+OH source, and only von Kuhlmann et al. (2003) quantified the contributions of other secondary pathways (including CH<sub>3</sub>O<sub>2</sub> + RO<sub>2</sub> and glycolaldehyde photolysis); <sup>f</sup>only Müller et al. (2016) separately accounted for this sink.

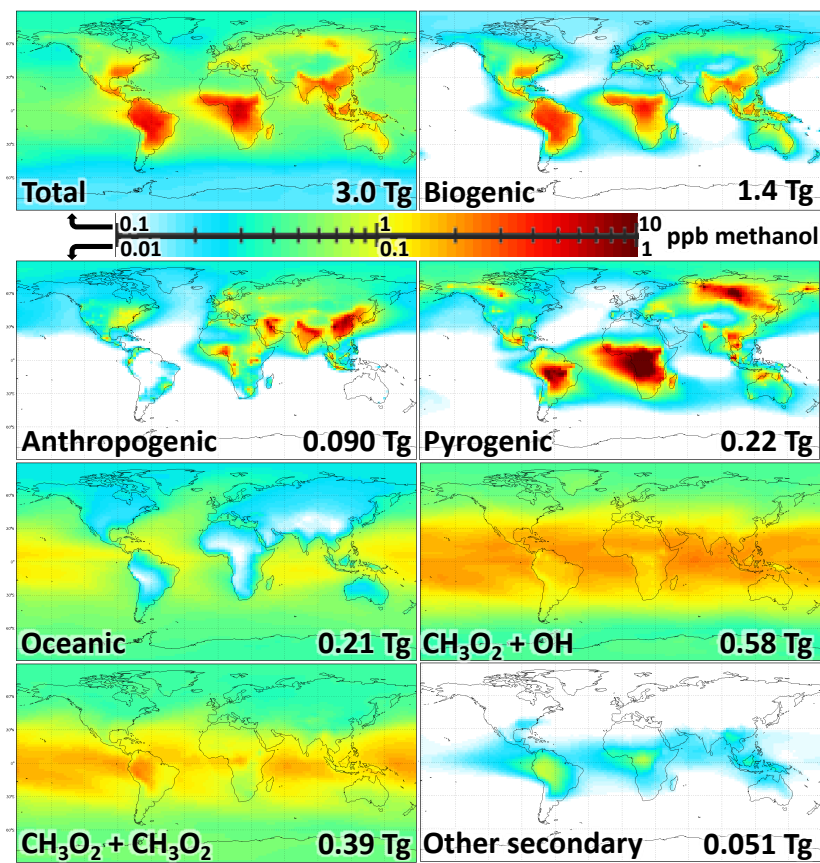


**Figure 6.** Methanol burden (top left) and contributions from individual sources. The maps shown annual average mixing ratios for the tropospheric column in the updated simulation. The scales for the total and biogenic panels differ from the others by a factor of ten. Numbers in the bottom right of each panel provide the annual average tropospheric burden of methanol from each source.

649 d) is much smaller than that of methanol from other sources (5.5 d); as a result, although  
 650 gross ocean emission provides 12% of the total atmospheric methanol source in our updated  
 651 simulation, it only contributes 7% of the tropospheric methanol burden.

### 652 5.1 Implications of methanol chemistry

653 Due to its ubiquity as the troposphere's most abundant non-methane VOC, methanol  
 654 can have important implications for the budgets of additional trace gases of interest. Fig-  
 655 ure 7 shows the changes in tropospheric OH, ozone, formaldehyde, and CO due to methanol  
 656 photochemistry, computed as the difference between simulations without and with the  
 657 methanol + OH and methanol + Cl reactions (using the updated methanol sources). Methanol  
 658 oxidation contributes 4.0% of the tropospheric CO burden and 4.8% of the formaldehyde  
 659 burden, and increases the surface ozone burden by 1.0%. It also causes a 0.9% reduc-  
 660 tion in tropospheric OH, thus augmenting the lifetime of other trace gases such as methane.

661 These impacts are not uniformly distributed throughout the atmosphere. For ex-  
 662 ample, the OH reduction due to methanol photooxidation is strongest in the boundary  
 663 layer (1.8%), and reaches up to 4% in areas with high biogenic methanol emissions. Con-  
 664 versely, due to its long lifetime against oxidation, methanol plays its most prominent role

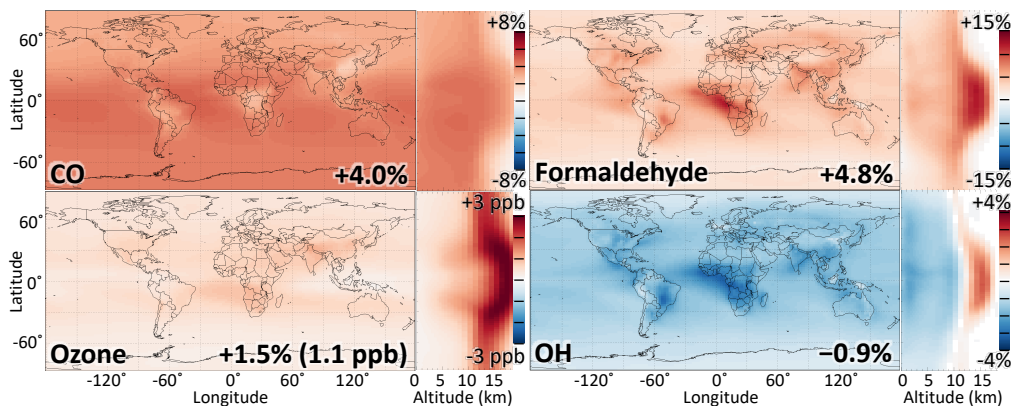


**Figure 7.** The role of methanol in trace gas budgets. Each panel shows changes in the annual column-average, zonal-average, and overall (numbers at bottom right) tropospheric burden of a select species due to the inclusion of methanol photochemistry in GEOS-Chem, computed by comparing the updated simulation to a sensitivity simulation in which methanol photooxidation is removed. The scale for ozone shows absolute changes in mixing ratio, while those for the other species are shown as percent changes.

665 in trace gas budgets in the tropical upper troposphere. There, methanol contributes up  
 666 to 14% of the formaldehyde burden; subsequent radical production from the photolysis  
 667 of this formaldehyde increases OH by 5%. More details on the spatial patterns of these  
 668 changes are given in Table S5, while Figure S10 shows the changes due solely to primary  
 669 methanol emissions, which are similar in pattern to those in Figure 7 but smaller in mag-  
 670 nitude.

671 Finally, the implementation of the  $\text{CH}_3\text{O}_2 + \text{OH}$  reaction in the GEOS-Chem chem-  
 672 ical mechanism alters tropospheric radical budgets, particularly over the tropical oceans  
 673 where the  $\text{CH}_3\text{O}_2$  lifetime is longest. The spatial patterns of these changes are shown  
 674 in Figure 8. Globally, the  $\text{CH}_3\text{O}_2 + \text{OH}$  reaction represents 14% of the fate of  $\text{CH}_3\text{O}_2$   
 675 radicals, behind only reaction with  $\text{NO}$  (44%) and  $\text{HO}_2$  (38%) in our updated simula-  
 676 tion. The direct consequences of this reaction are decreases in the annual average tropo-  
 677 spheric burdens of  $\text{CH}_3\text{O}_2$  and OH by 20% and 1.1% respectively, reaching local max-  
 678 ima of 45% and 7% in the tropical ocean boundary layer. These decreases have secondary  
 679 effects on the budgets of their other reaction partners, most notably  $\text{HO}_2$  and  $\text{NO}$ , whose  
 680 tropospheric burdens increase by 5.5% and 1.1% respectively (up to 14% and 11% lo-  
 681 cally). Additional impacts of the  $\text{CH}_3\text{O}_2 + \text{OH}$  reaction, including changes to formalde-  
 682 hyde, CO, ozone, and methyl hydroperoxide, are provided in Table S5 and Figure S11.

## 683 6 Conclusions

684 We have used observations from the ATom aircraft campaign over the Pacific and  
 685 Atlantic Oceans, simulated with source-tagged tracers in the GEOS-Chem model, to bet-  
 686 ter understand the factors controlling methanol concentrations in the remote oceanic at-  
 687 mosphere. From there we constructed a new global budget for methanol and examined  
 688 the implications for global atmospheric chemistry.

689 We find that background methanol concentrations in the remote oceanic atmosphere  
 690 (200-400 pptv) are mostly controlled by chemical production from the  $\text{CH}_3\text{O}_2 + \text{OH}$  and  
 691  $\text{CH}_3\text{O}_2 + \text{CH}_3\text{O}_2$  reactions (global sources of 33 and 24  $\text{Tg a}^{-1}$ , respectively). The  $\text{CH}_3\text{O}_2$   
 692 + OH reaction is generally not included in global models of atmospheric chemistry, but

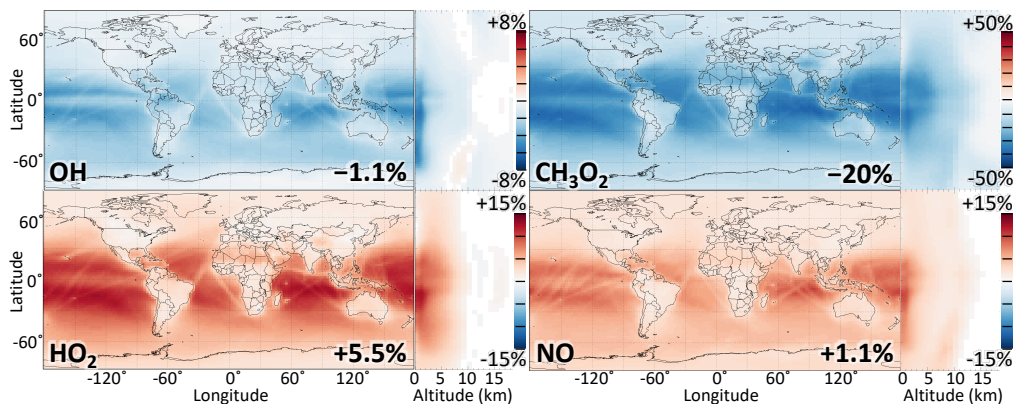


**Figure 8.** The role of the  $\text{CH}_3\text{O}_2 + \text{OH}$  reaction in radical budgets. Each panel shows changes in the annual column-average, zonal-average, and overall (number at bottom right) tropospheric burden of a select species due to the inclusion of the  $\text{CH}_3\text{O}_2 + \text{OH}$  reaction in GEOS-Chem, computed by comparing the updated simulation to a sensitivity simulation in which the reaction in question is removed.

693 our results indicate that it produces methanol with 13% yield and more broadly impacts  
 694 hydrogen oxide ( $\text{HO}_x$ ) radical budgets. Air-sea exchange is optimized with a surface ocean  
 695 methanol concentration of 61 nM, resulting in the ocean representing a weak net sink  
 696 ( $14 \text{ Tg a}^{-1}$ ). Contrary to previous results, we find that the gross ocean emission of methanol  
 697 (here  $24 \text{ Tg a}^{-1}$ ) does not control methanol concentrations in the marine atmosphere,  
 698 even in the boundary layer, because of rapid deposition and the role of chemical produc-  
 699 tion.

700 The ATom observations also included a number of anthropogenic and biomass burn-  
 701 ing plumes containing elevated methanol. From correlations with CO, we inferred global  
 702 anthropogenic and biomass burning emissions of  $6.3$  and  $13 \text{ Tg a}^{-1}$ , respectively, at the  
 703 high end of current estimates. The methanol relative enhancement in biomass burning  
 704 plumes did not significantly change over prolonged aging, suggesting that chemical pro-  
 705 duction in the plumes compensates for loss from oxidation.

706 The resulting global budget of methanol constructed from our analysis has a global  
 707 source of  $205 \text{ Tg a}^{-1}$  including  $101 \text{ Tg a}^{-1}$  from the terrestrial biosphere and  $60 \text{ Tg a}^{-1}$   
 708 from chemical production. Ocean, biomass burning, and anthropogenic activities are ad-  
 709 ditional minor sources. The global atmospheric lifetime of methanol is 5.3 days, with ox-  
 710 idation and deposition each contributing about half of the sink. The secondary source  
 711 from chemical production accounts for 29% of the global source of methanol but 34%  
 712 of the global burden because it is less sensitive to deposition than the others. Sensitiv-  
 713 ity simulations with GEOS-Chem show that accounting for methanol chemistry increases  
 714 global tropospheric CO, formaldehyde, and ozone by 4.0%, 4.8%, and 1.5% respectively,  
 715 and decreases global tropospheric OH by 0.9%. Methanol chemistry aside, including the  
 716  $\text{CH}_3\text{O}_2 + \text{OH}$  reaction in GEOS-Chem has significant impact on global budgets includ-  
 717 ing for OH ( $-1.1\%$ ),  $\text{CH}_3\text{O}_2$  ( $-20\%$ ),  $\text{HO}_2$  ( $+5.5\%$ ), and NO ( $+1.1\%$ ).

## 718 Acknowledgments

719 We thank Bruce Daube and Roisin Commane for the use of their CO data and their  
 720 helpful input. This work was supported by the US NSF Atmospheric Chemistry Pro-  
 721 gram, by the NASA Atmospheric Composition Modeling and Analysis Program, and by

722 the US EPA Science To Achieve Results Program. K.H.B. acknowledges additional sup-  
 723 port from the Harvard University Center for the Environment and the National Oceanic  
 724 and Atmospheric Administration’s Climate and Global Change Fellowship programs. D.B.M.,  
 725 X.C., and K.C.W. acknowledge support from the NASA Atmospheric Composition Cam-  
 726 paign Data Analysis and Modeling (ACCDAM) program (grant NNX14AP89G). This  
 727 material is based upon work supported by the National Center for Atmospheric Research,  
 728 which is a major facility sponsored by the National Science Foundation under Cooper-  
 729 ative Agreement No. 1852977. All ATom data used in this study can be accessed via [https://](https://daac.ornl.gov/ATOM/campaign/)  
 730 [daac.ornl.gov/ATOM/campaign/](https://daac.ornl.gov/ATOM/campaign/)

## 731 References

- 732 Akagi, S. K., Yokelson, R. J., Burling, I. R., Meinardi, S., Simpson, I., Blake, D. R.,  
 733 ... Weise, D. R. (2013). Measurements of reactive trace gases and variable  
 734 O<sub>3</sub> formation rates in some South Carolina biomass burning plumes. *Atmos.*  
 735 *Chem. Phys.*, *13*, 1141-1165. doi: 10.5194/acp-13-1141-2013
- 736 Akagi, S. K., Yokelson, R. J., Wiedinmyer, C., Alvarado, M. J., Reid, J. S., Karl, T.,  
 737 ... Wennberg, P. O. (2011). Emission factors for open and domestic biomass  
 738 burning for use in atmospheric models. *Atmos. Chem. Phys.*, *11*, 4039-4072.  
 739 doi: 10.5194/acp-11-4039-2011
- 740 Andreae, M. O. (2019). Emission of trace gases and aerosols from biomass burning –  
 741 an updated assessment. *Atmos. Chem. Phys.*, *19*, 8523-8546. doi: 10.5194/acp-  
 742 -19-8523-2019
- 743 Andreae, M. O., & Merlet, P. (2001). Emission of trace gases and aerosols from  
 744 biomass burning. *Global Biogeochem. Cy.*, *15*, 955-966. doi: 10.1029/  
 745 2000GB001382
- 746 Apel, E. C., Emmons, L. K., Karl, T., Flocke, F., Hills, A. J., Madronich, S., ...  
 747 Riemer, D. D. (2010). Chemical evolution of volatile organic compounds in  
 748 the outflow of the Mexico City Metropolitan area. *Atmos. Chem. Phys.*, *10*,  
 749 2353-2375. doi: 10.5194/acp-10-2353-2010
- 750 Apel, E. C., Hills, A. J., Lueb, R., Zindel, S., Eisele, S., & Riemer, D. D. (2003). A  
 751 fast-GC/MS system to measure C<sub>2</sub> to C<sub>4</sub> carbonyls and methanol aboard air-  
 752 craft. *J. Geophys. Res.: Atmos.*, *108*, D208794. doi: 10.1029/2002JD003199
- 753 Apel, E. C., Hornbrook, R. S., Hills, A. J., Blake, N. J., Barth, M. C., Wein-  
 754 heimer, A., ... Riemer, D. D. (2015). Upper tropospheric ozone produc-  
 755 tion from lightning NO<sub>x</sub>-impacted convection: Smoke ingestion case study  
 756 from the DC3 campaign. *J. Geophys. Res.: Atmos.*, *120*, 2505-2523. doi:  
 757 10.1002/2014JD022121
- 758 Archibald, A. T., Petit, A. S., Percival, C. J., Harvey, J. N., & Shallcross, D. E.  
 759 (2009). On the importance of the reaction between OH and RO<sub>2</sub> radicals.  
 760 *Atmos. Sci. Lett.*, *10*, 102-108. doi: 10.1002/asl.216
- 761 Arrieta, J. M., Duarte, C. M., Sala, M. M., & Dachs, J. (2016). Out of thin air: mi-  
 762 crobial utilization of atmospheric gaseous organics in the surface ocean. *Fron-*  
 763 *tiers Microbiol.*, *6*, 1566. doi: 10.3389/fmicb.2015.01566
- 764 Ashworth, K., Chung, S. H., McKinney, K. A., Liu, Y., Munger, J. W., Martin,  
 765 S. T., & Steiner, A. L. (2016). Modelling bidirectional fluxes of methanol  
 766 and acetaldehyde with the FORCAST canopy exchange model. *Atmos. Chem.*  
 767 *Phys.*, *16*, 15461-15484. doi: 10.5194/acp-16-15461-2016
- 768 Assaf, E., Sheps, L., Whalley, L., Heard, D., Tomas, A., Schoemaeker, C., &  
 769 Fittschen, C. (2017). The reaction between CH<sub>3</sub>O<sub>2</sub> and OH radicals: Product  
 770 yields and atmospheric implications. *Environ. Sci. Technol.*, *51*, 2170-2177.  
 771 doi: 10.1021/acs.est.6b06265
- 772 Assaf, E., Song, B., Tomas, A., Schoemaeker, C., & Fittschen, C. (2016). Rate  
 773 constant of the reaction between CH<sub>3</sub>O<sub>2</sub> radicals and OH radicals revisited. *J.*  
 774 *Phys. Chem. A*, *120*, 8923-8932. doi: 10.1021/acs.jpca.6b07704

- 775 Atkinson, R., Baulch, D. L., Cox, R. A., Crowley, J. N., Hampson, R. F., Hynes,  
776 R. G., . . . Subcommittee, I. (2006). Evaluated kinetic and photochemical data  
777 for atmospheric chemistry: Volume II - gas phase reactions of organic species.  
778 *Atmos. Chem. Phys.*, *6*, 3625-4055. doi: 10.5194/acp-6-3625-2006
- 779 Bader, W., Stavrou, T., Muller, J.-F., Reimann, S., Boone, C. D., Harrison, J. J.,  
780 . . . Mahieu, E. (2014). Long-term evolution and seasonal modulation of  
781 methanol above Jungfraujoch (46.5 °N, 8.0 °E): optimisation of the retrieval  
782 strategy, comparison with model simulations and independent observations.  
783 *Atmos. Meas. Tech.*, *7*, 3861-3872. doi: 10.5194/amt-7-3861-2014
- 784 Bates, K. H., & Jacob, D. J. (2019). A new model mechanism for atmospheric  
785 oxidation of isoprene: global effects on oxidants, nitrogen oxides, organic prod-  
786 ucts, and secondary organic aerosol. *Atmos. Chem. Phys.*, *19*, 9613-9640. doi:  
787 10.5194/acp-19-9613-2019
- 788 Beale, R., Dixon, J. L., Arnold, S. R., Liss, P. S., & Nightingale, P. D. (2013).  
789 Methanol, acetaldehyde, and acetone in the surface waters of the atlantic  
790 ocean. *J. Geophys. Res.: Oceans*, *118*, 5412-5425. doi: 10.1002/jgrc.20322
- 791 Beale, R., Dixon, J. L., Smyth, T. J., & Nightingale, P. D. (2015). Annual study  
792 of oxygenated volatile organic compounds in UK shelf waters. *Marine Chem.*,  
793 *171*, 96-106. doi: 10.1016/j.marchem.2015.02.013
- 794 Beale, R., Liss, P. S., Dixon, J. L., & Nightingale, P. D. (2011). Quantification of  
795 oxygenated volatile organic compounds in seawater by membrane inlet-proton  
796 transfer reaction/mass spectrometry. *Anal. Chim. Acta*, *706*, 128-134. doi:  
797 10.1016/j.aca.2011.08.023
- 798 Borbon, A., Gilman, J. B., Kuster, W. C., Grand, N., Chevaillier, S., Colomb, A.,  
799 . . . de Gouw, J. A. (2013). Emission ratios of anthropogenic volatile organic  
800 compounds in northern mid-latitude megacities: Observations versus emis-  
801 sion inventories in Los Angeles and Paris. *J. Geophys. Res.: Atmos.*, *118*,  
802 2041-2057. doi: 10.1002/jgrd.50059
- 803 Bossolasco, A., Faragó, E. P., Schoemaeker, C., & Fittscher, C. (2014). Rate con-  
804 stant of the reaction between CH<sub>3</sub>O<sub>2</sub> and OH radicals. *Chem. Phys. Lett.*,  
805 *593*, 7-13. doi: 10.1016/j.cplett.2013.12.052
- 806 Brewer, J. F., Fischer, E. V., Commane, R., Wofsy, S. C., Daube, B., Apel, E. C.,  
807 . . . Ravishankara, A. R. (2020). Evidence for an oceanic source of methyl  
808 ethyl ketone to the atmosphere. *Geophys. Res. Lett.*, *47*, e2019GL086045. doi:  
809 10.1029/2019GL086045
- 810 Bruns, E. A., Slowik, J. G., El Haddad, I., Kilic, D., Klein, F., Dommen, J., . . .  
811 Prévôt, A. S. H. (2017). Characterization of gas-phase organics using proton  
812 transfer reaction time-of-flight mass spectrometry: fresh and aged residen-  
813 tial wood combustion emissions. *Atmos. Chem. Phys.*, *17*, 705-720. doi:  
814 10.5194/acp-17-705-2017
- 815 Butkovskaya, N., Rayez, M.-T., Rayez, J.-C., Kukui, A., & Le Bras, G. (2009).  
816 Water vapor effect on the HNO<sub>3</sub> yields in the HO<sub>2</sub> + NO reaction: experi-  
817 mental and theoretical evidence. *J. Phys. Chem. A*, *113*, 11327-11342. doi:  
818 10.1021/jp811428p
- 819 Caravan, R. L., Khan, M. A. H., Zádor, J., Sheps, L., Antonov, I. O., Rotavera, B.,  
820 . . . Taatjes, C. A. (2018). The reaction of hydroxyl and methylperoxy radicals  
821 is not a major source of atmospheric methanol. *Nature Comm.*, *9*, 4343. doi:  
822 10.1038/s41467-018-06716-x
- 823 Chao, W., Jr-MinLin, J., Takahashi, K., Tomas, A., Yu, L., Kajii, Y., . . . Fittschen,  
824 C. (2019). Water vapor does not catalyze the reaction between methanol  
825 and OH radicals. *Angew. Chem. Int. Ed.*, *58*(15), 5013-5017. doi:  
826 10.1002/anie.201900711
- 827 Chen, Q., Schmidt, J. A., Shah, V., Jaeglé, L., Sherwen, T., & Alexander, B. (2017).  
828 Sulfate production by reactive bromine: Implications for the global sulfur  
829 and reactive bromine budgets. *Geophys. Res. Lett.*, *44*, 7069-7078. doi:

- 10.1002/2017GL073812
- 830  
831 Chen, X., Millet, D. B., Singh, H. B., Wisthaler, A., Apel, E. C., Atlas, E. L., ...  
832 Yuan, B. (2019). On the sources and sinks of atmospheric VOCs: an in-  
833 tegrated analysis of recent aircraft campaigns over North America. *Atmos.*  
834 *Chem. Phys.*, *19*, 9097-9123. doi: 10.5194/acp-19-9097-2019
- 835 de Gouw, J. A., Middlebrook, A. M., Warneke, C., Goldan, P. D., Kuster, W. C.,  
836 Roberts, J. M., ... Bates, T. S. (2005). Budget of organic carbon in a pol-  
837 luted atmosphere: results from the New England Air Quality Study in 2002. *J.*  
838 *Geophys. Res.: Atmos.*, *110*, D16305. doi: 10.1029/2004JD005623
- 839 de Gouw, J. A., Warneke, C., Stohl, A., Wollny, A. G., Brock, C. A., Cooper, O. R.,  
840 ... Lueb, A. (2006). Volatile organic compounds composition of merged and  
841 aged forest fire plumes from Alaska and western Canada. *J. Geophys. Res.:*  
842 *Atmos.*, *111*(D10), 303. doi: 10.1029/2005JD006175
- 843 Deng, W., Peng, L., Jiao, N., & Zhang, Y. (2018). Differential incorporation of  
844 one-carbon substrates among microbial populations identified by stable isotope  
845 probing from the estuary to South China Sea. *Sci. Reports*, *8*, 15378. doi:  
846 10.1038/s41598-018-33497-6
- 847 Dinasquet, J., Tirola, M., & Azam, F. (2018). Enrichment of bacterioplankton able  
848 to utilize one-carbon and methylated compounds in the coastal Pacific Ocean.  
849 *Frontiers in Marine Sci.*, *5*, 307. doi: 10.3389/fmars.2018.00307
- 850 Diskin, G. S., Podolske, J. R., Sachse, G. W., & Slate, T. A. (2002). Open-path air-  
851 borne tunable diode laser hygrometer. In A. Fried (Ed.), *Diode lasers and ap-*  
852 *plications in atmospheric sensing* (Vol. 4817, p. 196 - 204). SPIE. doi: 10  
853 .1117/12.453736
- 854 Dixon, J. L., Beale, R., & Nightingale, P. D. (2011a). Microbial methanol uptake  
855 in northeast Atlantic waters. *J. Int. Soc. Microbial Ecol.*, *5*, 704-716. doi: 10  
856 .1038/ismej.2010.169
- 857 Dixon, J. L., Beale, R., & Nightingale, P. D. (2011b). Rapid biological oxidation  
858 of methanol in the tropical Atlantic: significance as a microbial carbon source.  
859 *Biogeosci.*, *8*, 2707-2716. doi: 10.5194/bg-8-2707-2011
- 860 Dixon, J. L., & Nightingale, P. D. (2012). Fine-scale variability in methanol uptake  
861 and oxidation: from the microlayer to 1000 m. *Biogeosci.*, *9*, 2961-2972. doi:  
862 10.5194/bg-9-2961-2012
- 863 Dixon, J. L., Sargeant, S., Nightingale, P. D., & Colin Murrell, J. (2013). Gra-  
864 dients in microbial methanol uptake: productive coastal upwelling waters  
865 to oligotrophic gyres in the Atlantic Ocean. *ISME J.*, *7*, 568-580. doi:  
866 10.1038/ismej.2012.130
- 867 Dufour, G., Boone, C. D., Rinsland, C. P., & Bernath, P. F. (2006). First space-  
868 borne measurements of methanol inside aged southern tropical to mid-latitude  
869 biomass burning plumes using the ACE-FTS instrument. *Atmos. Chem. Phys.*,  
870 *6*, 3463-3470. doi: 10.5194/acp-6-3463-2006
- 871 Duncan, B. N., Logan, J. A., Bey, I., Megretskaia, I. A., Yantosca, R. M., Novelli,  
872 P. C., ... Rinsland, C. P. (2007). Global budget of CO, 19881997: source  
873 estimates and validation with a global model. *J. Geophys. Res.*, *112*, D22301.  
874 doi: 10.1029/2007JD008459
- 875 Eastham, S. D., & Jacob, D. J. (2017). Limits on the ability of global eulerian  
876 models to resolve intercontinental transport of chemical plumes. *Atmos. Chem.*  
877 *Phys.*, *17*, 2543-2553. doi: 10.5194/acp-17-2543-2017
- 878 Eastham, S. D., Weisenstein, D. K., & Barrett, S. R. (2014). Development and  
879 evaluation of the unified tropospheric-stratospheric chemistry extension (UCX)  
880 for the global chemistry-transport model GEOS-Chem. *Atmos. Environ.*, *89*,  
881 52-63. doi: 10.1016/j.atmosenv.2014.02.001
- 882 Fall, R., & Benson, A. A. (1996). Leaf methanol the simplest natural product from  
883 plants. *Trends Plant Sci.*, *1*, 296-301. doi: 10.1016/S1360-1385(96)88175-0
- 884 Ferracci, V., Heimann, I., Abraham, N. L., Pyle, J. A., & Archibald, A. T. (2018).

- 885 Global modelling of the total OH reactivity: investigations on the “missing”  
886 OH sink and its atmospheric implications. *Atmos. Chem. Phys.*, *18*, 7109-  
887 7129. doi: 10.5194/acp-18-7109-2018
- 888 Fischer, E. V., Jacob, D. J., Millet, D. B., Yantosca, R. M., & Mao, J. (2012). The  
889 role of the ocean in the global atmospheric budget of acetone. *Geophys. Res.*  
890 *Lett.*, *39*, L01807. doi: 10.1029/2011GL050086
- 891 Fisher, J. A., Atlas, E. L., Barletta, B., Meinardi, S., Blake, D. R., Thompson,  
892 C. R., ... Murray, L. T. (2018). Methyl, ethyl, and propyl nitrates: global  
893 distribution and impacts on reactive nitrogen in remote marine environments.  
894 *J. Geophys. Res.: Atmos.*, *123*, 12429-12451. doi: 10.1029/2018JD029046
- 895 Fittschen, C., Whalley, L. K., & Heard, D. E. (2014). The reaction of CH<sub>3</sub>O<sub>2</sub> radi-  
896 cals with OH radicals: a neglected sink for CH<sub>3</sub>O<sub>2</sub> in the remote atmosphere.  
897 *Environ. Sci. Technol.*, *48*, 7700-7701. doi: 10.1021/es502481q
- 898 Fukui, Y., & Doskey, P. V. (1998). Air-surface exchange of nonmethane organic  
899 compounds at a grassland site: Seasonal variations and stressed emissions. *J.*  
900 *Geophys. Res.: Atmos.*, *103*, 13153-13168. doi: 10.1029/98JD00924
- 901 Galbally, I. E., & Kirstine, W. (2002). The production of methanol by flowering  
902 plants and the global cycle of methanol. *J. Atmos. Chem.*, *43*, 195-229. doi: 10  
903 .1023/A:1020684815474
- 904 Giglio, L., Randerson, J. T., & van der Werf, G. R. (2013). Analysis of daily,  
905 monthly, and annual burned area using the fourth-generation global fire emis-  
906 sions database (GFED4). *J. Geophys. Res.: Biogeosci.*, *118*, 317-328. doi:  
907 10.1002/jgrg.20042
- 908 Giovannoni, S. J., Hayakawa, D. H., Tripp, H. J., Stingl, U., Givan, S. A., Cho,  
909 J.-C., ... Rappé, M. S. (2008). The small genome of an abundant  
910 coastal ocean methylotroph. *Environ. Microbiol.*, *10*, 1771-1782. doi:  
911 10.1111/j.1462-2920.2008.01598.x
- 912 Goldan, P. D., Trainer, M., Kuster, W. C., Parrish, D. D., Carpenter, J., Roberts,  
913 J. M., ... Fehsenfeld, F. C. (1995). Measurements of hydrocarbons, oxy-  
914 genated hydrocarbons, carbon monoxide, and nitrogen oxides in an urban  
915 basin in Colorado: Implications for emission inventories. *J. Geophys. Res.:*  
916 *Atmos.*, *100*, 22771-22783. doi: 10.1029/95JD01369
- 917 Guenther, A., Jiang, X., Heald, C. L., Sakulyanontvittaya, T., Duhl, T., Emmons,  
918 L. K., & Wang, X. (2012). The model of emissions of gases and aerosols  
919 from nature version 2.1 (megan 2.1): an extended and updated framework  
920 for modeling biogenic emissions [Journal Article]. *Geosci. Model Dev.*, *5*(6),  
921 1471-1492.
- 922 Guenther, A., Karl, T., Harley, P., Wiedinmyer, C., Palmer, P. I., & Geron, C.  
923 (2006). Estimates of global terrestrial isoprene emissions using megan (model  
924 of emissions of gases and aerosols from nature). *Atmos. Chem. Phys.*, *6*,  
925 3181-3210. doi: 10.5194/acp-6-3181-2006
- 926 Harley, P., Greenberg, J., Niinemets, U., & Guenther, A. (2007). Environmental  
927 controls over methanol emission from leaves. *Biogeosci.*, *4*, 1083-1099. doi: 10  
928 .5194/bg-4-1083-2007
- 929 Heikes, B. G., Chang, W., Pilson, M. E. Q., Swift, E., Singh, H. B., Guenther, A.,  
930 ... Brand, L. (2002). Atmospheric methanol budget and ocean implication.  
931 *Global Biogeochem. Cy.*, *16*, 80-1-80-13. doi: 10.1029/2002GB001895
- 932 Holzinger, R., Jordan, A., Hansel, A., & Lindinger, W. (2001). Methanol measure-  
933 ments in the lower troposphere near Innsbruck (47.16 °N; 11.24 °E), Austria.  
934 *Atmos. Environ.*, *35*, 2525-2532. doi: 10.1016/S1352-2310(00)00430-1
- 935 Holzinger, R., Williams, J., Salisbury, G., Klüpfel, T., de Reus, M., Traub, M.,  
936 ... Lelieveld, J. (2005). Oxygenated compounds in aged biomass burn-  
937 ing plumes over the Eastern Mediterranean: evidence for strong secondary  
938 production of methanol and acetone. *Atmos. Chem. Phys.*, *5*, 39-46. doi:  
939 10.5194/acp-5-39-2005

- 940 Hornbrook, R. S., Blake, D. R., Diskin, G. S., Fried, A., Fuelberg, H. E., Meinardi,  
941 S., ... Apel, E. C. (2011). Observations of nonmethane organic com-  
942 pounds during ARCTAS - part 1: biomass burning emissions and plume  
943 enhancements. *Atmos. Chem. Phys.*, *11*, 11103-11130. doi: 10.5194/  
944 acp-11-11103-2011
- 945 Jacob, D. J., Field, B. D., Li, Q., Blake, D. R., de Gouw, J., Warneke, C., ...  
946 Guenther, A. (2005). Global budget of methanol: constraints from at-  
947 mospheric observations. *J. Geophys. Res.: Atmos.*, *110*, D08303. doi:  
948 10.1029/2004JD005172
- 949 Jara-Toro, R. A., Hernández, F. J., Taccone, R. A., Lane, S. I., & Pino, G. A.  
950 (2017). Water catalysis of the reaction between methanol and OH at 294 K  
951 and the atmospheric implications. *Angew. Chem. Int. Ed.*, *56*, 2166-2170. doi:  
952 10.1002/anie.201612151
- 953 Johnson, M. T. (2010). A numerical scheme to calculate temperature and salinity  
954 dependent air-water transfer velocities for any gas. *Ocean Sci.*, *6*, 913-920. doi:  
955 10.5194/os-6-913-2010
- 956 Kameyama, S., Tanimoto, H., Inomata, S., Tsunogai, U., Ooki, A., Takeda, S., ...  
957 Uematsu, M. (2010). High-resolution measurement of multiple volatile or-  
958 ganic compounds dissolved in seawater using equilibrator inletproton transfer  
959 reaction-mass spectrometry (EIPTR-MS). *Marine Chem.*, *122*, 59-73. doi:  
960 10.1016/j.marchem.2010.08.003
- 961 Karl, T., Guenther, A., Spirig, C., Hansel, A., & Fall, R. (2003). Seasonal varia-  
962 tion of biogenic VOC emissions above a mixed hardwood forest in northern  
963 Michigan. *Geophys. Res. Lett.*, *30*, 2186. doi: 10.1029/2003GL018432
- 964 Karl, T., Harley, P., Emmons, L., Thornton, B., Guenther, A., Basu, C., ... Jardine,  
965 K. (2010). Efficient atmospheric cleansing of oxidized organic trace gases by  
966 vegetation. *Science*, *330*(6005), 816-819. doi: 10.1126/science.1192534
- 967 Karl, T., Harley, P., Guenther, A., Rasmussen, R., Baker, B., Jardine, K., & Nemitz,  
968 E. (2005). The bi-directional exchange of oxygenated VOCs between a loblolly  
969 pine (*pinus taeda*) plantation and the atmosphere. *Atmos. Chem. Phys.*, *5*,  
970 3015-3031. doi: 10.5194/acp-5-3015-2005
- 971 Karl, T., Potosnak, M., Guenther, A., Clark, D., Walker, J., Herrick, J. D., &  
972 Geron, C. (2004). Exchange processes of volatile organic compounds above  
973 a tropical rain forest: Implications for modeling tropospheric chemistry above  
974 dense vegetation. *J. Geophys. Res.*, *109*, D18306. doi: 10.1029/2004JD004738
- 975 Karl, T., Striednig, M., Graus, M., Hammerle, A., & Wohlfahrt, G. (2018). Ur-  
976 ban flux measurements reveal a large pool of oxygenated volatile organic  
977 compound emissions. *Proc. Natl. Acad. Sci.*, *115*(6), 1186-1191. doi:  
978 10.1073/pnas.1714715115
- 979 Khan, M., Cooke, M., Utembe, S., Archibald, A., Derwent, R., Jenkin, M., ... Shall-  
980 cross, D. (2015). Global analysis of peroxy radicals and peroxy radical-  
981 water complexation using the STOCHEM-CRI global chemistry and transport  
982 model. *Atmos. Environ.*, *106*, 278-287. doi: 10.1016/j.atmosenv.2015.02.020
- 983 Khan, M., Cooke, M., Utembe, S., Xiao, P., Derwent, R., Jenkin, M., ... Shall-  
984 cross, D. (2014). Reassessing the photochemical production of methanol  
985 from peroxy radical self and cross reactions using the STOCHEM-CRI  
986 global chemistry and transport model. *Atmos. Environ.*, *99*, 77-84. doi:  
987 10.1016/j.atmosenv.2014.09.056
- 988 Kirstine, W., Galbally, I., Ye, Y., & Hooper, M. (1998). Emissions of volatile organic  
989 compounds (primarily oxygenated species) from pasture. *J. Geophys. Res.: At-  
990 mos.*, *103*, 10605-10619. doi: 10.1029/97JD03753
- 991 Lamarque, J.-F., Bond, T. C., Eyring, V., Granier, C., Heil, A., Klimont, Z., ...  
992 van Vuuren, D. P. (2010). Historical (1850-2000) gridded anthropogenic and  
993 biomass burning emissions of reactive gases and aerosols: methodology and ap-  
994 plication. *Atmos. Chem. Phys.*, *10*, 7017-7039. doi: 10.5194/acp-10-7017-2010

- 995 Legreid, G., Lööv, J. B., Staehelin, J., Hueglin, C., Hill, M., Buchmann, B., ...  
 996 Reimann, S. (2007). Oxygenated volatile organic compounds (OVOCs) at an  
 997 urban background site in Zürich (Europe): Seasonal variation and source allo-  
 998 cation. *Atmos. Environ.*, *41*, 8409-8423. doi: 10.1016/j.atmosenv.2007.07.026
- 999 Lewis, A. C., Evans, M. J., Hopkins, J. R., Punjabi, S., Read, K. A., Purvis, R. M.,  
 1000 ... Parrington, M. (2013). The influence of biomass burning on the global  
 1001 distribution of selected non-methane organic compounds. *Atmos. Chem. Phys.*,  
 1002 *13*, 851-867. doi: 10.5194/acp-13-851-2013
- 1003 Li, L., Chen, Y., Zeng, L., Shao, M., Xie, S., Chen, W., ... Cao, W. (2014).  
 1004 Biomass burning contribution to ambient volatile organic compounds (VOCs)  
 1005 in the Chengdu-Chongqing Region (CCR), China. *Atmos. Environ.*, *99*, 403-  
 1006 410. doi: 10.1016/j.atmosenv.2014.09.067
- 1007 Liss, P., & Slater, P. (1974). Flux of gases across the air-sea interface. *Nature*, *247*,  
 1008 181-184. doi: 10.1038/247181a0
- 1009 MacDonald, R. C., & Fall, R. (1993). Detection of substantial emissions of methanol  
 1010 from plants to the atmosphere. *Atmos. Environ.*, *27*, 1709-1713. doi: 10.1016/  
 1011 0960-1686(93)90233-O
- 1012 Madronich, S., & Calvert, J. G. (1990). Permutation reactions of organic peroxy  
 1013 radicals in the troposphere. *J. Geophys. Res.*, *95*, 56975715. doi: 10.1029/  
 1014 JD095iD05p05697
- 1015 Magneron, I., Mellouki, A., Le Bras, G., Moortgat, G. K., Horowitz, A., & Wirtz,  
 1016 K. (2005). Photolysis and OH-initiated oxidation of glycolaldehyde un-  
 1017 der atmospheric conditions. *J. Phys. Chem. A*, *109*, 4552-4561. doi:  
 1018 10.1021/jp044346y
- 1019 Mao, H., Talbot, R., Nielsen, C., & Sive, B. (2006). Controls on methanol and ace-  
 1020 tone in marine and continental atmospheres. *Geophys. Res. Lett.*, *33*, L02803.  
 1021 doi: 10.1029/2005GL024810
- 1022 Mauzerall, D. L., Logan, J. A., Jacob, D. J., Anderson, B. E., Blake, D. R., Brad-  
 1023 shaw, J. D., ... Talbot, B. (1998). Photochemistry in biomass burning plumes  
 1024 and implications for tropospheric ozone over the tropical South Atlantic. *J.*  
 1025 *Geophys. Res.: Atmos.*, *103*(D7), 8401-8423. doi: 10.1029/97JD02612
- 1026 McManus, J. B., Nelson, D. D., Shorter, J. H., Jimenez, R., Herndon, S., Saleska,  
 1027 S., & Zahniser, M. (2005). A high precision pulsed quantum cascade laser  
 1028 spectrometer for measurements of stable isotopes of carbon dioxide. *J. Mod.*  
 1029 *Optics*, *52*, 2309-2321. doi: 10.1080/09500340500303710
- 1030 Millet, D. B., Baasandorj, M., Farmer, D. K., Thornton, J. A., Baumann, K., Bro-  
 1031 phy, P., ... Xu, J. (2015). A large and ubiquitous source of atmospheric formic  
 1032 acid. *Atmos. Chem. Phys.*, *15*, 6283-6304. doi: 10.5194/acp-15-6283-2015
- 1033 Millet, D. B., Jacob, D. J., Custer, T. G., de Gouw, J. A., Goldstein, A. H., Karl,  
 1034 T., ... Williams, J. (2008). New constraints on terrestrial and oceanic  
 1035 sources of atmospheric methanol. *Atmos. Chem. Phys.*, *8*, 6887-6905. doi:  
 1036 10.5194/acp-8-6887-2008
- 1037 Mincer, T. J., & Aicher, A. C. (2016). Methanol production by a broad phylogenetic  
 1038 array of marine phytoplankton. *PLOS ONE*, *11*, 1-17. doi: 10.1371/journal  
 1039 .pone.0150820
- 1040 Mu, M., Randerson, J. T., van der Werf, G. R., Giglio, L., Kasibhatla, P., Mor-  
 1041 ton, D., ... Wennberg, P. O. (2011). Daily and 3-hourly variability  
 1042 in global fire emissions and consequences for atmospheric model predic-  
 1043 tions of carbon monoxide. *J. Geophys. Res.: Atmos.*, *116*, D24303. doi:  
 1044 10.1029/2011JD016245
- 1045 Müller, J.-F., Liu, Z., Nguyen, V. S., Stavrakou, T., Harvey, J. N., & Peeters,  
 1046 J. (2016). The reaction of methyl peroxy and hydroxyl radicals as a  
 1047 major source of atmospheric methanol. *Nature Comm.*, *7*, 13213. doi:  
 1048 10.1038/ncomms13213
- 1049 Nemecek-Marshall, M., MacDonald, R. C., Franzen, J. J., Wojciechowski, C. L.,

- 1050 & Fall, R. (1995). Methanol emission from leaves (enzymatic detection  
1051 of gas-phase methanol and relation of methanol fluxes to stomatal con-  
1052 ductance and leaf development). *Plant Physiology*, *108*, 1359-1368. doi:  
1053 10.1104/pp.108.4.1359
- 1054 Nightingale, P. D., Malin, G., Law, C. S., Watson, A. J., Liss, P. S., Liddicoat,  
1055 M. I., ... Upstill-Goddard, R. C. (2000). In situ evaluation of air-sea gas ex-  
1056 change parameterizations using novel conservative and volatile tracers. *Global*  
1057 *Biogeochem. Cy.*, *14*, 373-387. doi: 10.1029/1999GB900091
- 1058 Olivier, J. G. J., Bouwman, A. F., Vandermaas, C. W. M., & Berdowski, J. J. M.  
1059 (1994). Emission Database for Global Atmospheric Research (EDGAR). *Envi-*  
1060 *ron. Monit. Assess.*, *31*, 93-106.
- 1061 Orlando, J. J., & Tyndall, G. S. (2012). Laboratory studies of organic peroxy  
1062 radical chemistry: an overview with emphasis on recent issues of atmospheric  
1063 significance. *Chem. Soc. Rev.*, *41*, 6294-6317.
- 1064 Paulot, F., Wunch, D., Crounse, J. D., Toon, G. C., Millet, D. B., DeCarlo, P. F.,  
1065 ... Wennberg, P. O. (2011). Importance of secondary sources in the atmo-  
1066 spheric budgets of formic and acetic acids. *Atmos. Chem. Phys.*, *11*, 1989-  
1067 2013. doi: 10.5194/acp-11-1989-2011
- 1068 Potter, C. S., Randerson, J. T., Field, C. B., Matson, P. A., Vitousek, P. M.,  
1069 Mooney, H. A., & Klooster, S. A. (1993). Terrestrial ecosystem production: A  
1070 process model based on global satellite and surface data. *Global Biogeochem.*  
1071 *Cy.*, *7*, 811-841. doi: 10.1029/93GB02725
- 1072 Ramachandran, A., & Walsh, D. A. (2015). Investigation of XoxF methanol dehy-  
1073 drogenases reveals new methylotrophic bacteria in pelagic marine and freshwa-  
1074 ter ecosystems. *FEMS Microbio. Ecol.*, *91*. doi: 10.1093/femsec/fiv105
- 1075 Randerson, J. T., Chen, Y., van der Werf, G. R., Rogers, B. M., & Morton, D. C.  
1076 (2012). Global burned area and biomass burning emissions from small fires. *J.*  
1077 *Geophys. Res.: Biogeosci.*, *117*, G04012. doi: 10.1029/2012JG002128
- 1078 Randerson, J. T., Thompson, M. V., Conway, T. J., Fung, I. Y., & Field, C. B.  
1079 (1997). The contribution of terrestrial sources and sinks to trends in the  
1080 seasonal cycle of atmospheric carbon dioxide. *Global Biogeochem. Cy.*, *11*,  
1081 535-560. doi: 10.1029/97GB02268
- 1082 Read, K. A., Carpenter, J., Arnold, S. R., Beale, R., Nightingale, P. D., Hop-  
1083 kins, J. B., ... Pickering, S. J. (2012). Multi-annual observations of acetone,  
1084 methanol and acetaldehyde in remote tropical atlantic air: Implications for  
1085 atmospheric OVOC budgets and oxidative capacity. *Environ. Sci. Technol.*,  
1086 *46*, 1102811039. doi: 10.1021/es302082p
- 1087 Rinsland, C. P., Mahieu, E., Chiou, L., & Herbin, H. (2009). First ground-based in-  
1088 frared solar absorption measurements of free tropospheric methanol (CH<sub>3</sub>OH):  
1089 Multidecade infrared time series from Kitt Peak (31.9 °N 111.6 °W): Trend,  
1090 seasonal cycle, and comparison with previous measurements. *J. Geophys. Res.*,  
1091 *114*, D04309. doi: 10.1029/2008JD011003
- 1092 Ruuskanen, T. M., Müller, M., Schnitzhofer, R., Karl, T., Graus, M., Bamberger, I.,  
1093 ... Hansel, A. (2011). Eddy covariance VOC emission and deposition fluxes  
1094 above grassland using PTR-TOF. *Atmos. Chem. Phys.*, *11*, 611-625. doi:  
1095 10.5194/acp-11-611-2011
- 1096 Safieddine, S. A., Heald, C. L., & Henderson, B. H. (2017). The global nonmethane  
1097 reactive organic carbon budget: A modeling perspective. *Geophys. Res. Lett.*,  
1098 *44*, 3897-3906. doi: 10.1002/2017GL072602
- 1099 Sander, S. P., Friedl, R. R., Golden, D. M., Kurylo, M. J., Moortgat, G. K., Wine,  
1100 P. H., ... Orkin, V. L. (2006). Chemical kinetics and photochemical data for  
1101 use in atmospheric studies: Evaluation number 15, JPL Publication 0225. *Jet*  
1102 *Propulsion Laboratory, Pasadena*.
- 1103 Sargeant, S. L., Murrell, J. C., Nightingale, P. D., & Dixon, J. L. (2016). Sea-  
1104 sonal variability in microbial methanol utilisation in coastal waters of the

- western English Channel. *Marine Ecol. Prog. Ser.*, 550, 53-64. doi:  
10.3354/meps11705
- Sherwen, T., Evans, M. J., Carpenter, L. J., Andrews, S. J., Lidster, R. T., Dix, B.,  
... Ordóñez, C. (2016). Iodine's impact on tropospheric oxidants: A global  
model study in GEOS-Chem. *Atmos. Chem. Phys.*, 16(2), 1161-1186. doi:  
10.5194/acp-16-1161-2016
- Sherwen, T., Schmidt, J. A., Evans, M. J., Carpenter, L. J., Großmann, K., East-  
ham, S. D., ... Ordóñez, C. (2016). Global impacts of tropospheric halogens  
(Cl, Br, I) on oxidants and composition in GEOS-Chem. *Atmos. Chem. Phys.*,  
16, 12239-12271. doi: 10.5194/acp-16-12239-2016
- Simpson, I. J., Akagi, S. K., Barletta, B., Blake, N. J., Choi, Y., Diskin, G. S.,  
... Blake, D. R. (2011). Boreal forest fire emissions in fresh Canadian  
smoke plumes: C<sub>1</sub>-C<sub>10</sub> volatile organic compounds (VOCs), CO<sub>2</sub>, CO, NO<sub>2</sub>,  
NO, HCN and CH<sub>3</sub>CN. *Atmos. Chem. Phys.*, 11(13), 6445-6463. doi:  
10.5194/acp-11-6445-2011
- Singh, H. B., Chen, Y., Tabazadeh, A., Fukui, Y., Bey, I., Yantosca, R., ... Kondo,  
Y. (2000). Distribution and fate of selected oxygenated organic species in  
the troposphere and lower stratosphere over the atlantic. *J. Geophys. Res.:*  
*Atmos.*, 105, 3795-3805. doi: 10.1029/1999JD900779
- Singh, H. B., Tabazadeh, A., Evans, M. J., Field, B. D., Jacob, D. J., Sachse, G., ...  
Brune, W. H. (2003). Oxygenated volatile organic chemicals in the oceans:  
Inferences and implications based on atmospheric observations and air-sea  
exchange models. *Geophys. Res. Lett.*, 30, 1862. doi: 10.1029/2003GL017933
- Sinha, P., Hobbs, P. V., Yokelson, R. J., Bertschi, I. T., Blake, D. R., Simpson, I. J.,  
... Novakov, T. (2003). Emissions of trace gases and particles from savanna  
fires in southern Africa. *J. Geophys. Res.: Atmos.*, 108(D13), 8487. doi:  
10.1029/2002JD002325
- Sinha, P., Hobbs, P. V., Yokelson, R. J., Blake, D. R., Gao, S., & Kirchstet-  
ter, T. W. (2004). Emissions from miombo woodland and dambo grass-  
land savanna fires. *J. Geophys. Res.: Atmos.*, 109(D11), 305. doi:  
10.1029/2004JD004521
- Stavrakou, T., Guenther, A., Razavi, A., Clarisse, L., Clerbaux, C., Coheur, P.-F.,  
... Müller, J.-F. (2011). First space-based derivation of the global atmo-  
spheric methanol emission fluxes. *Atmos. Chem. Phys.*, 11, 4873-4898. doi:  
10.5194/acp-11-4873-2011
- Talbot, R., Mao, H. T., & Sive, B. (2005). Diurnal characteristics of surface level  
O<sub>3</sub> and other important trace gases in New England. *J. Geophys. Res.*, 110,  
D09307. doi: 10.1029/2004JD005449
- Thames, A. B., Brune, W. H., Miller, D. O., Allen, H. M., Apel, E. C., Blake, D. R.,  
... Wolfe, G. M. (2020). Missing OH reactivity in the global marine boundary  
layer. *Atmos. Chem. Phys.*, 20, 4013-4029. doi: 10.5194/acp-20-4013-2020
- Tie, X., Guenther, A., & Holland, E. (2003). Biogenic methanol and its im-  
pacts on tropospheric oxidants. *Geophys. Res. Lett.*, 30, 1881. doi:  
10.1029/2003GL017167
- Travis, K. R., Heald, C. L., Allen, H. M., Apel, E. C., Arnold, S. R., Blake, D. R.,  
... Yu, F. (2020). Constraining remote oxidation capacity with atom observa-  
tions. *Atmos. Chem. Phys. Discuss.*, 2020, 1-41. doi: 10.5194/acp-2019-931
- Tyndall, G. S., Cox, R. A., Granier, C., Lesclaux, R., Moortgat, G. K., Pilling,  
M. J., ... Wallington, T. J. (2001). Atmospheric chemistry of small  
organic peroxy radicals. *J. Geophys. Res.*, 106, 12157-12182. doi:  
10.1029/2000JD900746
- Vaida, V. (2011). Perspective: water cluster mediated atmospheric chemistry. *J.*  
*Chem. Phys.*, 135, 020901. doi: 10.1063/1.3608919
- van der Werf, G. R., Randerson, J. T., Giglio, L., Collatz, G. J., Mu, M., Ka-  
sibhatla, P. S., ... van Leeuwen, T. T. (2010). Global fire emissions

- and the contribution of deforestation, savanna, forest, agricultural, and peat fires (1997-2009). *Atmos. Chem. Phys.*, *10*, 11707-11735. doi: 10.5194/acp-10-11707-2010
- Velasco, E., Pressley, S., Grivicke, R., Allwine, E., Coons, T., Foster, W., ... Lamb, B. (2009). Eddy covariance flux measurements of pollutant gases in urban Mexico City. *Atmos. Chem. Phys.*, *9*, 7325-7342. doi: 10.5194/acp-9-7325-2009
- von Dahl, C. C., Hvecker, M., Schlögl, R., & Baldwin, I. T. (2006). Caterpillar-elicited methanol emission: a new signal in plant-herbivore interactions? *Plant J.*, *46*, 948-960. doi: 10.1111/j.1365-3113.2006.02760.x
- von Kuhlmann, R., Lawrence, M. G., Crutzen, P. J., & Rasch, P. J. (2003). A model for studies of tropospheric ozone and nonmethane hydrocarbons: model evaluation of ozone-related species. *J. Geophys. Res.*, *108*, 4729. doi: 10.1029/2002JD003348
- Wang, S., Apel, E. C., Schwantes, R. H., Bates, K. H., Jacob, D. J., Fischer, E. V., ... Wofsy, S. C. (2020). Global atmospheric budget of acetone: air-sea exchange and the contribution to the hydroxyl radicals. *J. Geophys. Res.: Atmos.*, *In Review*.
- Wang, S., Hornbrook, R. S., Hills, A., Emmons, L. K., Tilmes, S., Lamarque, J.-F., ... Apel, E. C. (2019). Atmospheric acetaldehyde: importance of air-sea exchange and a missing source in the remote troposphere. *Geophys. Res. Lett.*, *46*, 5601-5613. doi: 10.1029/2019GL082034
- Wang, Y., Logan, J. A., & Jacob, D. J. (1998). Global simulation of tropospheric O<sub>3</sub>-NO<sub>x</sub>-hydrocarbon chemistry: 2. model evaluation and global ozone budget. *J. Geophys. Res.: Atmos.*, *103*, 10727-10755. doi: 10.1029/98JD00157
- Warneke, C., Bahreini, R., Brioude, J., Brock, C. A., de Gouw, J. A., Fahey, D. W., ... Veres, P. (2009). Biomass burning in Siberia and Kazakhstan as an important source for haze over the Alaskan Arctic in April 2008. *Geophys. Res. Lett.*, *36*(L02), 813. doi: 10.1029/2008GL036194
- Warneke, C., Karl, T., Judmaier, H., Hansel, A., Jordan, A., Lindinger, W., & Crutzen, P. (1999). Acetone, methanol, and other partially oxidized volatile organic emissions from dead plant matter by abiological processes: Significance for atmospheric HO<sub>x</sub> chemistry. *Global Biogeochem. Cy.*, *13*, 9-17. doi: 10.1029/98GB02428
- Warneke, C., McKeen, S. A., de Gouw, J. A., Goldan, P. D., Kuster, W. C., Holloway, J. S., ... Blake, D. R. (2007). Determination of urban volatile organic compound emission ratios and comparison with an emissions database. *J. Geophys. Res.: Atmos.*, *112*, D10S47. doi: 10.1029/2006JD007930
- Wells, K. C., Millet, D. B., Cady-Pereira, K. E., Shephard, M. W., Henze, D. K., Bousserez, N., ... Singh, H. B. (2014). Quantifying global terrestrial methanol emissions using observations from the TES satellite sensor. *Atmos. Chem. Phys.*, *14*, 2555-2570. doi: 10.5194/acp-14-2555-2014
- Wells, K. C., Millet, D. B., Hu, L., Cady-Pereira, K. E., Xiao, Y., Shephard, M. W., ... Sive, B. C. (2012). Tropospheric methanol observations from space: retrieval evaluation and constraints on the seasonality of biogenic emissions. *Atmos. Chem. Phys.*, *12*, 5897-5912. doi: 10.5194/acp-12-5897-2012
- Wennberg, P. O., Bates, K. H., Crounse, J. D., Dodson, L. G., McVay, R. C., Mertens, L. A., ... Seinfeld, J. H. (2018). Gas-phase reactions of isoprene and its major oxidation products. *Chem. Rev.*, *118*, 3337-3390. doi: 10.1021/acs.chemrev.7b00439
- Wentworth, G. R., Aklilu, Y.-A., Landis, M. S., & Hsu, Y.-M. (2018). Impacts of a large boreal wildfire on ground level atmospheric concentrations of PAHs, VOCs and ozone. *Atmos. Environ.*, *178*, 19-30. doi: 10.1016/j.atmosenv.2018.01.013
- Williams, J., Holzinger, R., Gros, V., Xu, X., Atlas, E., & Wallace, D. W. R. (2004).

- 1215 Measurements of organic species in air and seawater from the tropical Atlantic.  
1216 *Geophys. Res. Lett.*, *31*, L23S06. doi: 10.1029/2004GL020012
- 1217 Wohl, C., Brown, I., Kitidis, V., Jones, A. E., Sturges, W. T., Nightingale, P. D.,  
1218 & Yang, M. (2020). Underway seawater and atmospheric measurements of  
1219 volatile organic compounds in the Southern Ocean. *Biogeosci.*, *17*, 2593-2619.  
1220 doi: 10.5194/bg-17-2593-2020
- 1221 Wohlfahrt, G., Amelynck, C., Ammann, C., Arneht, A., Bamberger, I., Goldstein,  
1222 A. H., . . . Schoon, N. (2015). An ecosystem-scale perspective of the net land  
1223 methanol flux: synthesis of micrometeorological flux measurements. *Atmos.*  
1224 *Chem. Phys.*, *15*, 7413-7427. doi: 10.5194/acp-15-7413-2015
- 1225 Yan, C., Kocevskaja, S., & Krasnoperov, L. N. (2016). Kinetics of the reaction of  
1226  $\text{CH}_3\text{O}_2$  radicals with OH studied over the 292-526 K temperature range. *J.*  
1227 *Phys. Chem. A*, *120*, 6111-6121. doi: 10.1021/acs.jpca.6b04213
- 1228 Yan, C., & Krasnoperov, L. N. (2019). Pressure-dependent kinetics of the reac-  
1229 tion between  $\text{CH}_3\text{O}_2$  and OH: TRIOX formation. *J. Phys. Chem. A*, *123*,  
1230 8349-8357. doi: 10.1021/acs.jpca.9b03861
- 1231 Yang, M., Beale, R., Liss, P., Johnson, M., Blomquist, B., & Nightingale, P. (2014).  
1232 Air-sea fluxes of oxygenated volatile organic compounds across the Atlantic  
1233 Ocean. *Atmos. Chem. Phys.*, *14*, 7499-7517. doi: 10.5194/acp-14-7499-2014
- 1234 Yang, M., Blomquist, B. W., & Nightingale, P. D. (2014b). Air-sea exchange  
1235 of methanol and acetone during HiWinGS: Estimation of air phase, water  
1236 phase gas transfer velocities. *J. Geophys. Res.: Oceans*, *119*, 7308-7323. doi:  
1237 10.1002/2014JC010227
- 1238 Yang, M., Nightingale, P. D., Beale, R., Liss, P. S., Blomquist, B., & Fairall, C.  
1239 (2013). Atmospheric deposition of methanol over the Atlantic Ocean. *Proc.*  
1240 *Natl. Acad. Sci.*, *110*, 20034-20039. doi: 10.1073/pnas.1317840110
- 1241 Zhuang, J., Jacob, D. J., & Eastham, S. D. (2018). The importance of vertical res-  
1242 olution in the free troposphere for modeling intercontinental plumes. *Atmos.*  
1243 *Chem. Phys.*, *18*, 6039-6055. doi: 10.5194/acp-18-6039-2018